UPPSALA
UNIVERSITET

Examensarbete 15 hp
Juni 2016

Future directions in the study of Asymptotic Giant Branch Stars with the James Webb Space Telescope

Adam Hjort

Kandidatprogrammet i Fysik

Department of Physics and Astronomy

UPPSALA
UNIVERSITET

Teknisk- naturvetenskaplig fakultet
UTH-enheten

Besöksadress:
Ångströmlaboratoriet
Lägerhyddsvägen 1
Hus 4, Plan 0

Postadress:
Box 536
751 21 Uppsala

Telefon:
018 – 471 30 03

Telefax:
018 – 471 30 00

Hemsida:
http://www.teknat.uu.se/student

Abstract

Future directions in the study of Asymptotic Giant Branch Stars with the James Webb Space Telescope

Adam Hjort

English
In this study we present photometric predictions for C-type Asymptotic Giant Branch Stars (AGB) stars from Eriksson et al. (2014) for the James Webb Space Telescope (JWST) and the Wide-field Infrared Survey Explorer (WISE) instruments. The photometric predictions we have done are for JWST's general purpose wide-band filters on NIRCam and MIRI covering wavelengths of 0.7 — 21 microns. AGB stars contribute substantially to the integrated light of intermediate-age stellar populations and is a substantial source of the metals (especially carbon) in galaxies. Studies of AGB stars are (among other reasons) important for the understanding of the chemical evolution and dust cycle of galaxies. Since the JWST is scheduled for launch in 2018 it should be a high priority to prepare observing strategies. With these predictions we hope it will be possible to optimize observing strategies of AGB stars and maximize the science return of JWST. By testing our method on Whitelock et al. (2006) objects from the WISE catalog and comparing them with our photometric results based on Eriksson et al. (2014) we have been able to fit 20 objects with models.
The photometric data set can be accessed at:
http://www.astro.uu.se/AGBmodels/

Svenska
I den här studien har jag gjort fotometriska förutsägelser för asymptotiska jättegrensstjärnor (AGB-stjärnor) av C typ från Eriksson et al. (2014) modifierade för instrument ombord på James Webb Space Telescope (JWST) och Wide-field Infrared Survey Explorer (WISE). AGB-stjärnor bidrar kraftigt till det totala ljuset av stjärnor av intermediär ålder och är också en stor källa till metaller (speciellt kol) i galaxer. Studier av AGB stjärnor är viktiga av flera anledningar, däribland för att förstå den kemiska evolutionen och stoftcykler i galaxer. JWST är planerad att skjutas upp 2018 och fram till dess bör det vara en hög prioritet att förbereda observeringsstrategier. Med den fotometriska datan i den här studien hoppas vi att användare av JWST kommer kunna optimera sina observeringsstrategier av AGB-stjärnor och få ut så mycket som möjligt av sin obseravtionstid med teleskopet. Vi har testat metoden genom att titta på objekt från Whitelock et al. (2006) i WISE-katalogen och jämföra dem med de fotometriska resultaten baserade på modellerna från Eriksson et al. (2014). På detta sett har vi lyckats matcha 20 objekt med modeller.
Den fotometriska datan går att ladda ner ifrån:
http://www.astro.uu.se/AGBmodels/

Handledare: Erik Zackrisson
Ämnesgranskare: Sofia Ramstedt
Examinator: Gabriella Andersson

Contents

Chapter 1

Introduction

In this study we have calculated synthetic photometry for carbon rich AGB stars using several filter systems including filter systems for the upcoming space observatory James Webb Space Telescope. The motivation behind the work is to provide future users of JWST with a catalogue of a wide range of models and their photometric fluxes to help the users plan their observing strategies. The models we have used are from Eriksson, K. et al. (2014) and are of a type known as DARWIN (Dynamic Atmosphere & Radiation-driven Wind models based on Implicit Numerics) described in more detail in Höfner et al. (2016). To test our results we have looked at objects from Whitelock et al. (2006) in the AllWISE Multiepoch Photometry Database and matched them to the closest corresponding model.

Chapter 2

Background

2.1 Stellar evolution & AGB stars

The AGB phase is a late stage in stellar evolution undertaken by stars with a mass of $0.6 - 10M_{\odot}$. During the AGB phase the star start to burn helium in a shell around the core, into carbon and it also loses a significant fraction ($10^{-9} - 10^{-4}$ $M_{\odot}$ year^{-1}) of its mass due to strong stellar winds (Prialnik, 2009). The ejected material eventually mixes into the interstellar medium. AGB stars contribute substantially to the integrated light of intermediate-age stellar populations and is a substantial source of the metals (especially carbon) in galaxies. Studies of AGB stars are (among other reasons) important for the understanding of the chemical evolution and dust cycle of galaxies.

2.1.1 The main sequence

A very common plot when studying stars is the so called Hertzsprung–Russell (H-R) diagram created by astronomers Ejnar Hertzsprung and Henry Norris Russell in the early twentieth century. There exist several different ways to portray the diagram but the key point is to plot the star's luminosity (or absolute magnitude) versus the stars effective temperature (or their spectral classifications). Doing this for many stars yields a plot where several distinct regions becomes apparent. An example of an H-R diagram can be found in Figure 2.1. Most of the lifetime of a star is spent burning hydrogen on the main sequence. The main sequence is the horizontal region going from the upper left to the lower right in Figure 2.1. In stars with mass $\lesssim 1.3M_{\odot}$, the dominant process in which hydrogen is converted into helium is the proton-proton (p-p) chain. The p-p chain consists of three paths in which hydrogen nuclei (i.e. protons) are converted into helium. It always starts with two protons fusing and forming deuterium:

$$p + p \rightarrow ^2\mathrm{D} + e^+ + \nu \tag{2.1}$$

The deuterium then fuses with another proton which creates Helium-3:

$$^2\mathrm{D} + p \rightarrow ^3\mathrm{He} + \gamma \tag{2.2}$$

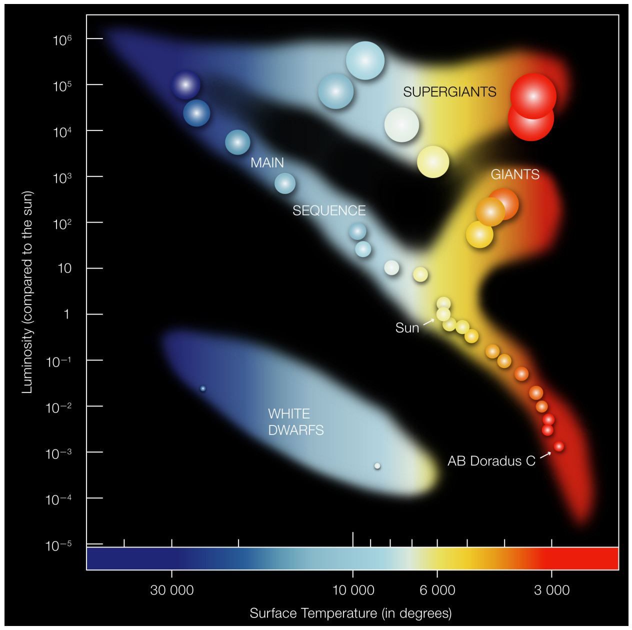

Figure 2.1: A typical HR diagram. Credit: ESO (2007)

Next there are two different paths that the chain can take, either the helium-3 can fuse with another helium-3 which completes the p-p I chain:

$$^3\text{He} + ^3\text{He} \rightarrow ^4\text{He} + 2p \tag{2.3}$$

Alternatively the helium-3 can fuse with helium-4 and create beryllium:

$$^3\text{He} + ^4\text{He} \rightarrow ^7\text{Be} + \gamma \tag{2.4}$$

The beryllium can either capture an electron which creates lithium which then can capture a proton making two helium-4 nuclei. This is the end of the p-p II chain:

$$\begin{gathered} ^7\text{Be} + e^- \rightarrow ^7\text{Li} + \nu \\ ^7\text{Li} + p \rightarrow 2\,^4\text{He} \end{gathered} \tag{2.5}$$

Instead of an electron the beryllium can capture a proton which will create the radioactive isotope boron-8 that decays into the unstable isotope beryllium-8 before almost instantly decaying into two helium-4 nuclei. This marks the end of the p-p III chain:

$$\begin{gathered} ^7\text{Be} + p \rightarrow ^8\text{B} + \gamma \\ ^8\text{B} \rightarrow ^8\text{Be} + e^+ + \nu \\ ^8\text{Be} \rightarrow 2\,^4\text{He} \end{gathered} \tag{2.6}$$

Inside a star all three paths of the chain occur simultaneously and which path that dominates is dependent on the temperature, density and abundances of the different elements involved (Prialnik, 2009).

In stars that are slightly more massive than the sun ($\gtrsim 1.3M_\odot$) the dominant hydrogen-burning fusion process is the CNO-cycle. CNO is an abbreviation for carbon, nitrogen and oxygen and these elements and fluorine are the participants in a series of reactions that converts hydrogen into helium. A schematic overview of the CNO-cycle can be seen in Figure 2.2. The AGB stars that this study is about lies in the mass range of 0.6 - $10M_\odot$ so both the p-p chain and the CNO-cycle occurs. Eventually the star will run out of hydrogen to burn in the core and begin to wander off the main sequence. The final fate of a star depends on the star's mass. The most massive stars end their lives in a supernova explosion, leaving a neutron star or a black hole. The fate of the low- and intermediate-mass stars that are covered by this study will be discussed in the following sections.

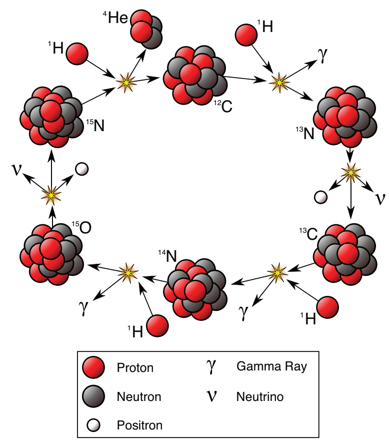

Figure 2.2: Illustration showing the processess involved in the CNO-cycle. Credit: Wikimedia Commons (2006)

2.1.2 Leaving the main sequence

When a main sequence star in the mass range 0.6 - $10M_\odot$ has burned the hydrogen in its core the thermal equilibrium is destroyed. The star now burns hydrogen in a shell around the core and swells up to become a red giant, moving to the right in the Hertzsprung–Russell diagram (see Figure 2.3a) onto the Red Giant Branch (RGB). The cores mass continues to grow as helium from the burning of hydrogen in the surrounding shell is added to the core and the core contracts, raising its temperature. The stars outer layers starts to expand which leads to cooling of the effective temperature and an increase in luminosity. The star is now a red giant. During the red giant phase convection zones in the star reaches deep enough to bring products created by the stellar nucleosynthesis up to the surface which changes the composition in the photosphere. The ratio of carbon-12 to nitrogen-14 will be lowered since carbon-12 gets draged inwards whereas nitrogen-14 is transported outwards. Other ratios such as carbon-12 to carbon-13 and lithium to helium-3 will also be altered. This process is known as the first dredge-up (Carroll and Ostlie, 2014). Eventually the temperature in the core is high enough (10^8 K) for the helium core to ignite and start the 3α-process, converting helium into carbon and oxygen by first fusing two helium-4 into beryllium-8. But as was mentioned in Section 2.1.1 beryllium-8 quickly decays back into two helium-4 nucleus. However the mean collision time is, due to the high temperature in the core, lower than the decay time which means that there is a small probability (Prialnik, 2009) for another helium-4 nucleus to collide with the short-lived beryllium-8 creating the stable isotope carbon-12:

$$\begin{aligned} {}^4\mathrm{He} + {}^4\mathrm{He} &\rightleftharpoons {}^8\mathrm{Be} \\ {}^8\mathrm{Be} + {}^4\mathrm{He} &\rightarrow {}^{12}\mathrm{C} \end{aligned} \tag{2.7}$$

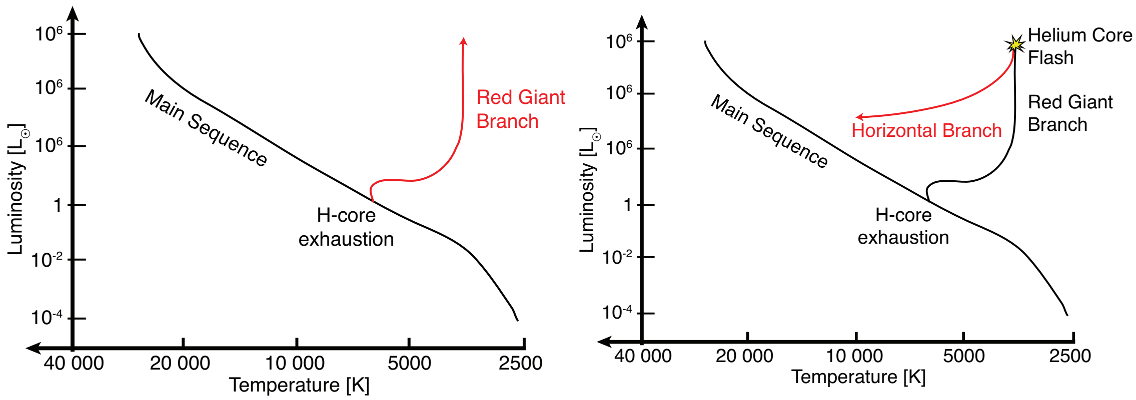

(a) Illustration showing the evolutionary path for a sun-like star leaving the main sequence and reaching the Red Giant Branch.

(b) Illustration showing the evolutionary path for a sun-like star moving onto Horisontal Branch after the helium core flash.

Figure 2.3: Based on work by: NOAO/AURA/NSF (2003)

And through α-capture, carbon-12 can create oxygen-16:

$$^{12}\text{C} + ^{4}\text{He} \rightarrow ^{16}\text{O} \tag{2.8}$$

For stars in the range 0.6 - $2M_\odot$ the electrons in the helium core have become degenerate before helium-burning can start. When the temperature is high enough for helium-burning to start, the star will undergo runaway nuclear fusion of helium. This event is known as a helium core flash. The core temperature will rise, the degeneracy will cease, the helium-burning will stabilize and the core will expand. For more massive stars the start of helium-burning is more gentle. The outer layers will now contract and the effective temperature will increase. The star will now move to the left in the Hertzsprung–Russell diagram on what is called the horizontal branch (see Figure 2.3b).

2.1.3 Early Asymptotic Giant Branch

Eventually the core is converted into a mixture of carbon and oxygen (CO) and helium burns in a shell around it. Much like when entering the red giant branch the star now starts moving upwards to the right in the HR-diagram (see Figure 2.4b) on the Asymptotic Giant Branch (AGB). Hydrogen also continues to burn in a shell above the helium shell that encapsulates the core. The two-shell burning is a characteristic trait of AGB stars and an illustration of this can be seen in Figure 2.4a. The helium-burning in the shell makes the CO core contract which makes the higher layer expand and cool. The lower temperature in the higher layers leads to a stop of the fusion processes in the hydrogen-burning shell. Because of the lower temperature in the envelope, the convection zones can reach even deeper into the star and drag up helium and nitrogen (Carroll and Ostlie, 2014). This event is known as the second dredge-up.

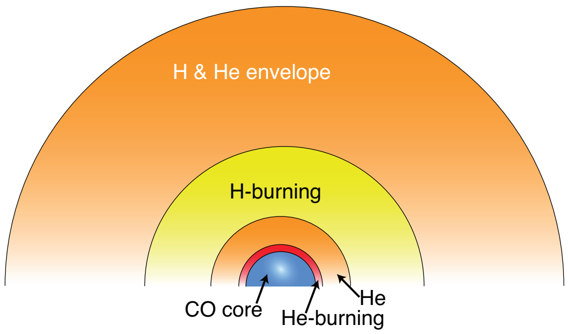

(a) Illustration showing the different shells inside an AGB star. Note that the shells are not to scale.

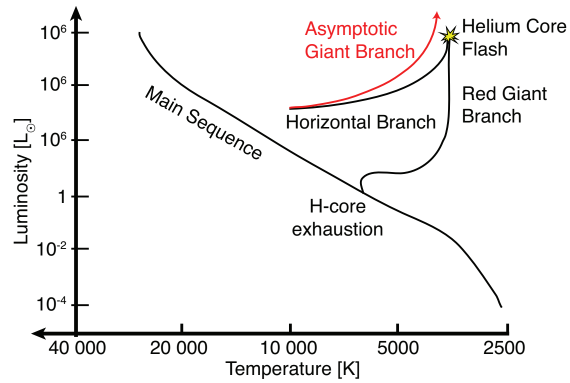

(b) Illustration showing the evolutionary path for a sun-like star leaving the horizontal branch and entering the Asymptotic Giant Branch. Based on work by: NOAO/AURA/NSF (2003)

Figure 2.4

2.1.4 Thermally-pulsing Asymptotic Giant Branch

Eventually the temperature in the hydrogen shell will have risen enough to reactivate the hydrogen-burning shell and become the dominant source for the stars energy output. When the hydrogen burns the resulting helium ashes fall down and add up on the underlying helium shell. The increased mass of the helium shell makes the region closest to the core degenerate and the helium-burning stops. Like in the helium core flash discussed in Section 2.1.2 the temperature will eventually be high enough for the helium-burning to start which results in a runaway burning known as a helium shell flash. The energy output from the helium shell flash is absorbed by the hydrogen-burning shell, making it expand and cool leading to a turn off of the hydrogen-burning shell. The temperature in the hydrogen shell rises over time until it is high enough for hydrogen-burning to start again. This process repeats over and over with a period ranging from $10^2 - 10^5$ years depending on the mass of the star (Prialnik, 2009). The lower the mass is the longer is the time between pulses (Carroll and Ostlie, 2014). Because of the long periods it is not possible to observe a full pulsation. After a pulse the stellar parameters are almost the same as before the flash occurred but with slightly greater luminosity and slightly lower effective temperature. Another interesting characteristic of AGB stars is that the luminosity no longer depends on the total stellar mass but solely on the mass of the core. The luminosity for an AGB star can be described with the relation (Prialnik, 2009):

$$\frac{L}{L_\odot} = 6 \times 10^4 \left(\frac{M_\mathrm{c}}{M_\odot} - 0.5 \right) \tag{2.9}$$

Where L is the luminosity of the star being investigated, $L_\odot$ is the luminosity of the sun, M_c is the mass of the stars core and $M_\odot$ is the mass of the sun.

During a flash, a convection zone is created that stretches between the hydrogen-burning shell and the helium-burning shell. There is also strong convection present in the envelope. The depth of the envelope convection zone reaches deeper after each pulsation and for stars with a mass $> 2M_{\odot}$ the zones can mix which leads to the third dredge-up. In the third dredge-up mainly carbon created in the CNO cycle is brought up to the surface of the star. If the ratio of carbon to oxygen observed in the star's spectra is greater than unity the star is called a carbon star, or C-star for short. Along with carbon there are also so called s-process products being brought to the surface. S-process nucleosynthesis is caused by neutron capture. In the CNO-cycle free neutrons are produced and because neutrons are not charged they don't have to, as opposed to the situation in α-capture, overcome the Coulomb barrier to be captured. This can build up a quite heavy nucleus, however a radioactive isotope will eventually form and depending on the supply of free neutrons it may β^{-}-decay before another neutron can be captured. Since the half-life for the unstable isotopes is fixed, the probability for a β^{-}-decay is not affected by the surrounding environment, whereas the probability for neutron capture is affected by both the temperature and density of the surrounding (Prialnik, 2009). If the neutron capture occurs slower than the β^{-}-decay, the isotope decays before it can capture a neutron which is called an s-process. If the neutron capture occurs more rapidly than the decay time it is called an r-process. An example of an s-process product is technetium-99 which has a half life of 211 000 years before decaying into the stable ruthenium-99. Since technetium-99 have been observed in the stellar atmosphere of AGB stars the best explanation is that it has been created recently through the s-process inside the star before being brought to the surface during the third dredge-up (Carroll and Ostlie, 2014).

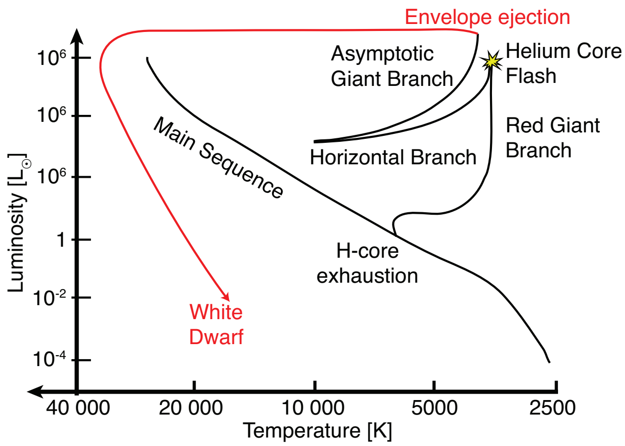

(a) Illustration showing the evolutionary path for a sun-like star shedding its envelope and becoming a white dwarf.
Based on work by: NOAO/AURA/NSF (2003)

(b) Photo of M27 - a planetary nebula.
Credit: Hjort and Holmberg (2015)

Figure 2.5

2.1.5 Post Asymptotic Giant Branch

A third characteristic of AGB stars is their rapid mass loss due to strong stellar winds driven by radiation pressure. The outer layers of AGB stars are cool enough for atoms to form molecules which in turn can form very small dust particles. The dust enshrouds the star creating a circumstellar envelope (CSE). The dust, and gas dragged along with the dust, is ejected with the winds where it eventually mixes with the interstellar medium. The dynamics of stellar winds is very complex thus making it very hard and computationally expensive to make accurate models and the processes that drives it is not fully understood. Observations suggests that the typical mass loss lies in the range $10^{-9}\,M_\odot - 10^{-4}\,M_\odot$ year^{-1} (Prialnik, 2009). The winds get stronger and eventually a superwind will develop and the entire envelope of the star is ejected leaving the baren CO-core. The ejected envelope form a nebula around the core. These are due to historical reasons called planetary nebulas although they have nothing to do with planets. A photo of a planetary nebula - M27 (also known as the Dumbbell Nebula) can be seen in Figure 2.5b. The planetary nebula colors is a result of UV radiation emitted by the core being absorbed by the gas and remitted at optical wavelengths Carroll and Ostlie (2014). In about 50 000 years the planetary nebula will dissipate into the interstellar medium and the only thing left will be the CO electron-degenerate core which is now classified as a white Dwarf which will cool during millions of years until its luminosity is so low that it will fade into a black dwarf (Prialnik, 2009).

2.2 James Webb Space Telescope

The JWST is an upcoming space observatory operated by NASA, ESA, CSA and STScl with a planned launch in October 2018 aboard an Ariane 5 ECA rocket from French Guiana. The telescope is often referred to as the successor to the Hubble Space Telescope (HST) although Hershel Space Observatory or Spitzer Space Telescope are more closely related in terms of wavelength range. JWST will feature a 6.5 meter segmented gold coated beryllium mirror. This mirror is so big that their currently is no rocket with the cargo capacity to to carry such a payload. Therefore the telescope is folded inside the rocket's cargo bay as can be seen in Figure 2.6. It will then unfold during the journey toward its destination: Sun-Earth Lagrange point 2. The destination, usually denoted L2 for short, lies roughly 1.5 million km from earth (more than three times the distance to the moon) and is chosen because here the telescope can orbit both the sun and be in a stable configuration with respect to its position relative earth without the need to consume huge amounts of fuel. An illustration of how JWST will look in space can be seen in Figure 2.7. Because of the far away distance it will not be possible to do any future reparations or upgrades as was possible with the HST. From launch it is estimated to take about six months of calibrations before the first science missions can begin. The whole mission is planed to work at least five years but hopefully ten years. What is special about JWST compared to HST except the size of its mirror is that it is built to be extremely sensitive at near-to-mid infrared wavelengths whereas HST operates mainly in UV to near infrared wavelengths. When observing in infrared several cosmic objects that are hidden behind dust in optical wavelengths become visible. Also objects which lie at very high redshifts becomes accessible when observing in infrared. This is because the objects move away from us with velocities that have increased the wavelengths of the light emitted from the objects making them appear "redder" (hence the name redshift) until they are practically only visible to us in infrared. There are four core science goals that JWST have been built to investigate (NASA/STScI, 2016a):

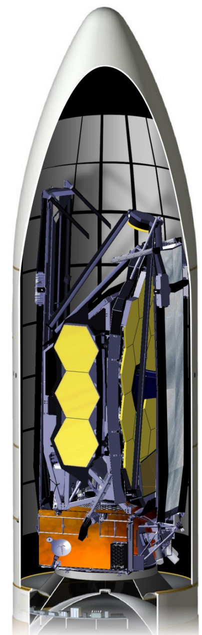

Figure 2.6: Illustration showing JWST folded inside an Ariane 5 rocket. Credit: Arianespace - ESA - NASA (2009)

- First light — finding the first galaxies and stars that formed in the universe
- Assembly of Galaxies — Investigate how galaxies have formed and evolved by observing the oldest high redshift galaxies
- Stellar and planetary formation — Being able to peek through the dust that enshrouds protostars JWST will give new insights into how stars and planets are born.
- Exoplanets — By studying the atmospheres of exoplanets JWST will search for the building blocks of life.

Besides the above mentioned core goals JWST will of course also be an excellent tool to study dust enshrouded AGB stars (Meixner, 2011).

The JWST will carry four main scientific instruments: the Near-Infrared Camera (NIRCam), the Near-Infrared Spectrograph (NIRSpec), the Mid-Infrared Instrument (MIRI) and the Guidance Sensor/ Near InfraRed Imager and Slitless Spectrograph (FGS/NIRISS). All instruments will be incorporated together in the Integrated Science Instrument Module (ISIM) located behind the primary mirror. NIRCam is the primary imager on JWST and features a mercury-cadmium-telluride (also known as H2RG) sensor that is sensitive in the range 0.6 — 5 microns. NIRCam is equipped with a total of 29 filters - 2 extra wide-band, 8 wide-band, 12 medium- band and 7 narrow-band filters (NASA/STScI, 2016c). It also have a coronagraph allowing it to block out strong light sources when observing faint objects. MIRI is equipped with an arsenic doped silicon sensor sensitive in the 5 — 28 micron range. MIRI have 10 wide-band imaging filters and 8 filters used for special applications (NASA/STScI, 2016b). The photometric predictions we have done in this study are for the general purpose wide-band filters on NIRCam and MIRI covering wavelengths of 0.7 — 21 microns.

The huge mirror in combination with these state-of-the-art instruments will provide unprecedented high resolution data and will most likely lead to many new discoveries about our universe.

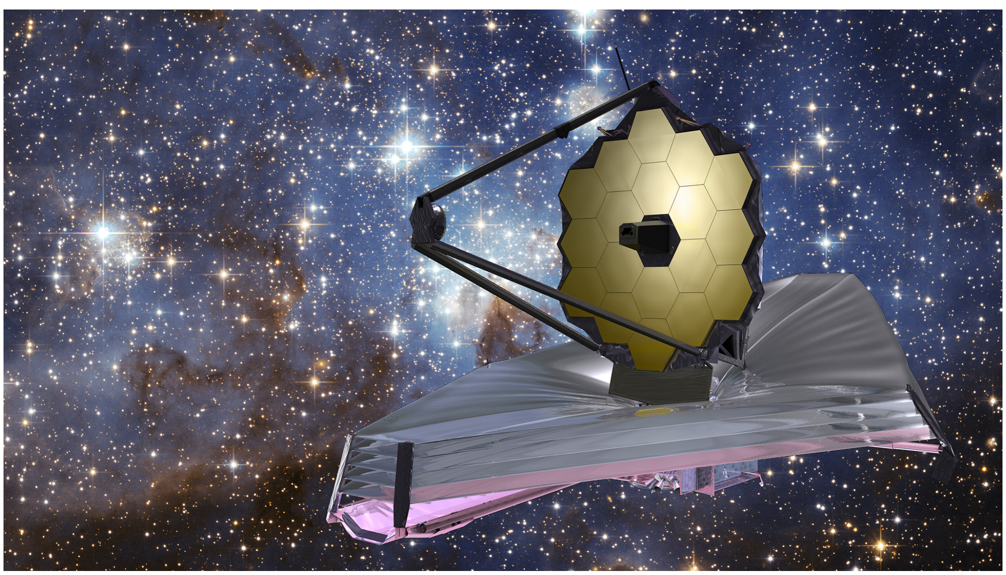

Figure 2.7: Montage of JWST in space. Credit: Northrop Grumman & ESA/Hubble (2006)

Chapter 3

Method

3.1 Photometry

There exist several methods of observing stars and depending on what is being investigated the methods carry different advantages. Spectroscopy can tell many things about a star and its chemical composition, but is compared to photometry a very time consuming process. When using photometry the star's flux is observed in several filters and by comparing the flux in the different filters certain parameters can be determined. A common way to present the fluxes are to plot the flux versus the wavelength in what is known as a Spectral Energy Distribution (SED) plot. Several SEDs are presented in Chapter 4. Filters are divided into different categories depending on how wide their transmission profile is, all the filters used in this study are so called wide-band filters. There exist many different filter systems and in this study the eight general purpose wide-band filters on NIRCam covering wavelengths from $0.7-4.4$ microns as well as eight of the imaging filters on MIRI covering wavelengths in the range of $5.6-21$ microns have been used. The data has also been processed using the WISE filter system covering $3.3-21.9$ microns and a generic filter system (UX BX B V R I J J_{2MASS} H H_{2MASS} Ks_{2MASS} K L L' M M') used in Eriksson, K. et al. (2014) covering $0.4-4.8$ microns. An overview of the filters used and their effective wavelength (i.e. the wavelength where it is easiest for photons to pass through, denoted λ_{eff}) is available in Appendix A. The transmission curves for the filter systems can be seen in Figure 3.1.

3.2 The grid

In the paper *An extensive grid of dynamic atmosphere and wind models* by Eriksson, K. et al. (2014), a grid of 540 dynamical models of C-type AGB stars have been computed using advanced models executed on supercomputers. A grid is the name used when describing an ensemble of models calculated using the same code but with varying stellar parameters. A table showing the span of parameters covered by the models can be found in Appendix B.1. Describing all the steps involved in creating a grid is beyond the scope of this study but it requires solving a set of equations describing the hydrodynamics, frequency-dependent

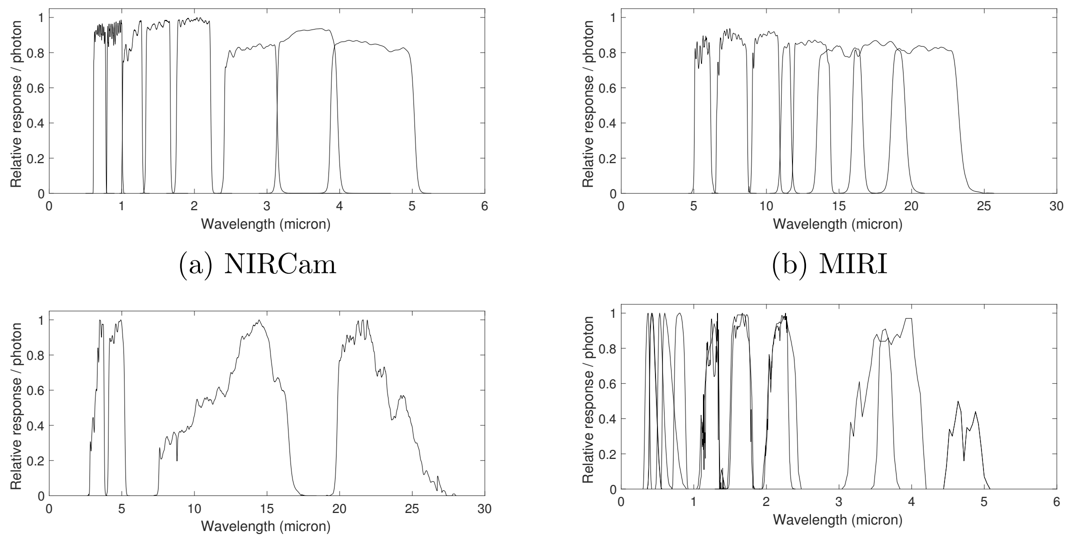

(a) NIRCam

(b) MIRI

(c) WISE

(d) UX BX B V R I J J_{2MASS} H H_{2MASS} Ks_{2MASS} K L L' M M'

Figure 3.1: Transmission curves for the different filter systems used throughout this study.

radiative transfer, and dust formation (assuming spherical symmetry). These equations are coupled, meaning that they need to be solved simultaneously (Eriksson, K. et al., 2014). The result is a catalogue of low resolution spectra. Due to dynamical instability in the photosphere AGB stars are so called long-period variable stars (LPV), meaning that their luminosity varies with periods of 100-1000 of days (not to be confused with the extremely long luminosity variations caused by thermal instabilities which have much longer periods as was discussed in Section 2.1.4). Because of the variation in luminosity each model contains between 1 to 5 epochs containing time-series spectra for different stages of pulsations in the model. In total there are 67 808 spectra that could be used for this study. Because of the huge number of individual files the first thing developed was a MATLAB code that automatically could scan the folders for their content before processing the data.

3.3 Processing spectra

The way to process a spectrum starts with loading a raw spectrum into MATLAB. The raw spectrum is given as two columns where one contains the wavelength in Ångström and the other the corresponding flux given in the units erg s^{-1} (denoted νL_ν). The flux is then divided with the corresponding wavelength (λ_f) in Ångström:

$$\mathbf{f}_\lambda = \frac{\nu L_\nu}{\boldsymbol{\lambda}_f} \quad [\mathrm{erg\,s^{-1}\mathring{A}^{-1}}] \tag{3.1}$$

The transmission curve for the first filter for the chosen filter system is loaded. The transmission curves are also given in two columns - the first one for the wavelength given in

Ångström ($\boldsymbol{\lambda}_T$) and the second for the transmission at that wavelength. The transmission is a dimensionless number for the probability that a photon will pass through the filter at a particular wavelength (usually given in a scale of 0-1 or 0-100). The spectrum and the transmission wavelength data is then converted into into units of Hz:

$$\boldsymbol{\nu}_f = \frac{c}{\left(\boldsymbol{\lambda}_f \times 10^{-10}\right)} \quad [\mathrm{Hz}] \tag{3.2}$$

Where c is the speed of light in m/s.

$$\boldsymbol{\nu}_T = \frac{c}{\left(\boldsymbol{\lambda}_f \times 10^{-10}\right)} \quad [\mathrm{Hz}] \tag{3.3}$$

Next the spectrum data in $\mathbf{f}_\lambda$ is converted into units of erg s^{-1} cm^{-2} Å^{-1}:

$$\mathbf{f}_\nu = \frac{\mathbf{f}_\lambda \times 10^{10}\left(\boldsymbol{\lambda}_f \times 10^{-10}\right)^2}{c\,4\pi\,(1000\text{ pc})^2} \quad [\mathrm{erg\,s^{-1}cm^{-2}\text{Å}^{-1}}] \tag{3.4}$$

Where the 1000 pc term in the denominator is needed for the unit switch to work and to scale the spectrum into a more convenient format. The spectrum and transmission curve are then interpolated to be at the same frequency scale using MATLABs `interp1` function. To use this function $\Delta\nu_T$ must first be set:

$$\Delta\nu_T = \frac{(\max(\boldsymbol{\nu}_T) - \min(\boldsymbol{\nu}_T))}{(\mathrm{int} - 1)} \tag{3.5}$$

Where *int* is the number of points the data will be interpolated into. In this study we have set *int* to be 10 000. Finally the AB magnitudes for the spectrum is calculated:

$$M_{AB} = -2.5\log_{10}\left(\frac{\sum(\mathbf{f}_\nu\boldsymbol{\nu}_T)\Delta\nu}{\sum(\boldsymbol{\nu}_T)\Delta\nu}\right) - 48.6 \quad [\mathrm{erg\,s^{-1}cm^{-2}Hz^{-1}}] \tag{3.6}$$

The code for how this is done can be found in Appendix C.1.2. This process is then repeated for the next filter in the filter system until all filters are done. The MATLAB code has been written so that both a single model as well as a span of models can be processed. The results are saved in tab delimited .dat files and the user gets the option to save plots of the result. Once a model has been computed the results can be viewed as an animation showing how the SED and the colours will change during an epoch.

3.4 Extracting objects from the WISE catalogue

Since JWST is not due for launch until 2018 it is not yet possible to test the accuracy of the results on data from JWST. As an alternative way to test the result we have looked in the WISE catalogue *AllWISE Multiepoch Photometry Database* and tried to fit the results to C-stars presented in Whitelock et al. (2006). Objects in the WISE catalogue are given in apparent Vega magnitudes (denoted m_{Vega}). Vega magnitudes are a different magnitude system where the star Vega is defined to have a 0 magnitude whereas AB magnitudes is an absolute system based on SI units. The Vega magnitudes given in the WISE data needs to be converted into absolute AB magnitudes. This is done by first converting the apparent AB magnitudes using the relation:

$$m_{\text{AB}} = m_{\text{Vega}} + \Delta m \tag{3.7}$$

Where Δm is given as

Band	Δm
W1	2.699
W2	3.319
W3	5.242
W4	6.604

Table 3.1: Values of Δm to convert Vega magnitudes to AB magnitudes in the WISE bands (IPAC/Caltech, 2012)

The next step is to convert the WISE data from apparent to absolute magnitudes, this is done using the relation

$$M_{\text{AB}} = m_{\text{AB}} + 5 - 5\log_{10} d - A \tag{3.8}$$

Where d is the distance in pc and A is the extinction. Both d and A is available in Whitelock et al. (2006), however the extinction does not have the same effect in the infrared wavelengths as in the V band for which the extinctions are given. An online tool by Doug Welch based on an algorithm developed by Cardelli et al. (1989) is used to estimate the extinction. We assume that the extinctions given from Whitelock et al. (2006) only affects data in W1 and can be neglected for the other bands.

The detector on WISE is very sensitive and luminous objects tend to saturate the sensor. An example of this can be seen in Figure 3.2 where the luminous carbon star CW Leo have saturated the sensor. When selecting objects from Whitelock et al. (2006) the first task is to check if the object is saturated before proceeding. An example of an object that passed the saturation test is [TI98]0418+0122 that can be seen in Figure 3.3. Of the 239 objects presented in Whitelock et al. (2006) only 26 had not saturated the sensor and could be used for further processing.

Since the data from WISE are multi-epoch there exist several observations of the same object and the next step is to filter out the observations that for various reason are not good enough to be used. This is done by eliminating all observations that doesn't contain data for all bands and where the observations have an $\chi^2_{\text{red}} > 5$. The code used for this is found in Appendix C.2.2. After the data that could not be used had been removed, 20 objects remained. The final 20 objects are presented in Appendix D.1. The final step is to find which model corresponds best to the observations. To solve this task a program was written

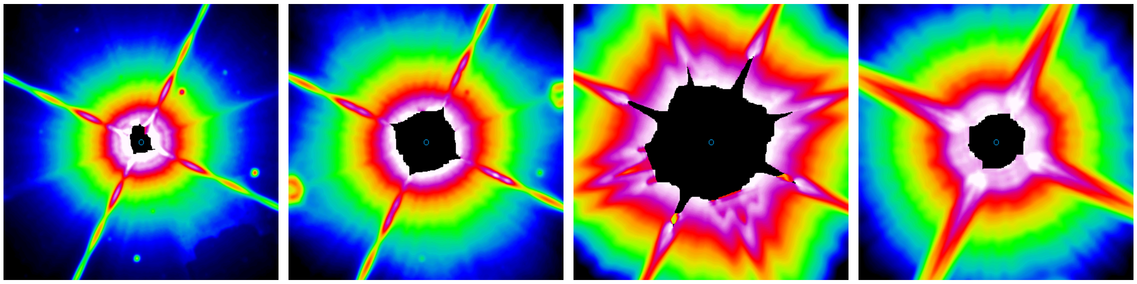

(a) W1 (b) W2 (c) W3 (d) W4

Figure 3.2: CW Leo as observed by WISE.

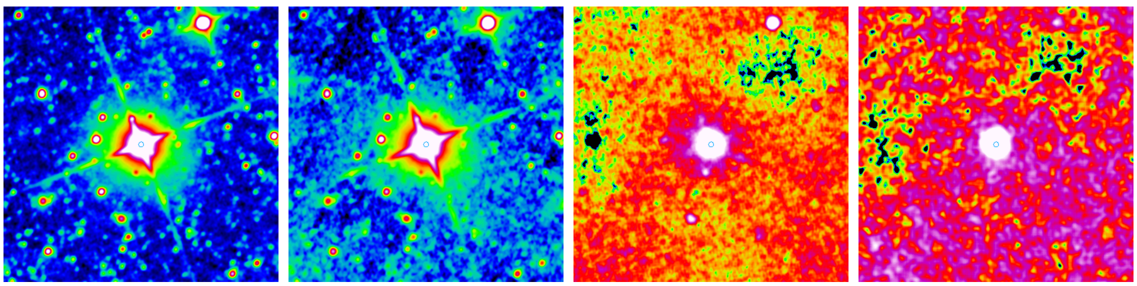

(a) W1 (b) W2 (c) W3 (d) W4

Figure 3.3: [TI98]0418+0122 as observed by WISE.

in MATLAB that can be found in Appendix C.2.1. The program works by minimizing each observation against each models and finding the model that gives the closest value to zero. After this have been done for all observations the program checks if any model was fitted to more than one observation. If this is the case the most frequent model is selected. Otherwise the model from the list of potential models that gave the closest value to zero is selected. Example of fitting a model to the data: Object A has 3 good observations (A_1, A_2, A_3). To each observation a model is fitted and the value for how much that model deviates from the observation is recorded. If each observation gets matched to a unique model the one that deviates the least is chosen as the best fit. If however for example both A_1 and A_3 gets assigned the same model that is consider a better fit even if the model assigned to A_2 had the least deviation. The best is of course a combination of the two scenarios where the model with least deviation is assigned to different observations. The program then presents the user with a plot of the best fit and a plot of all spectra for that model and all the observations for the object. Finally information about the object and the model are saved to a .txt file.

Chapter 4

Results

The result of this study is divided into two parts. First we present a catalogue of photometric fluxes in NIRCam, MIRI, WISE and a generic filter system, second we present the result from the extracted WISE objects from Whitelock et al. (2006).

4.1 Extracted WISE objects

The objects from Whitelock et al. (2006) that have been matched with a model SED are presented later in this chapter with plots showing the fit and information about the model. Model classes are explained in Appendix B.2. On the last page in this chapter table 4.2 is presented that gives the observed and the model magnitudes for the different objects. Below in Table 4.1 we present a comparison of the mass loss rate for objects where this was available in both the model information and in Whitelock et al. (2006).

Number	**Object Name**	$\mathbf{log\dot{M}_{obs}}$	$\mathbf{log\dot{M}_{mod}}$
1	[TI98]0418+0122	-5.73	-5.70
2	V617 Mon	-5.96	-5.14
14	[ABC89]Cen32	-5.45	-4.94
20	[TI98]2223+2548	-5.94	-5.75

Table 4.1: List of objects where mass loss was avaliable for both the model and the object in Whitelock et al. (2006). The mass loss rate is given in $M_{\odot}$/year

4.2 Photometric fluxes

Due to the very large size (more than 270 000 rows of data) of these results it is for practical reason not possible to present them directly in this study. Instead the result have been made available online at `http://www.astro.uu.se/AGBmodels/`. An example of how the results can be visualized is available in Figure 4.1.

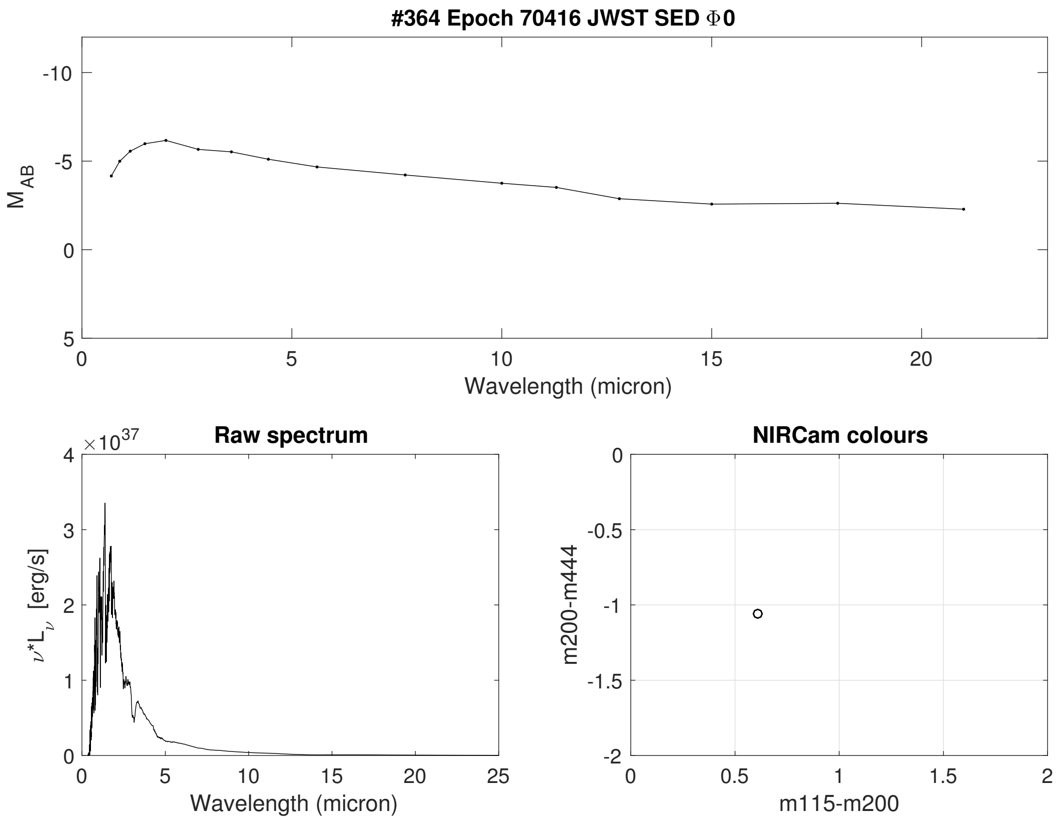

Figure 4.1: Example of photometric result in JWST showing the SED, NIRCam colours and the raw spectra. Model 364 - The best fitted model for object #19 - [TI98]2259+1249.

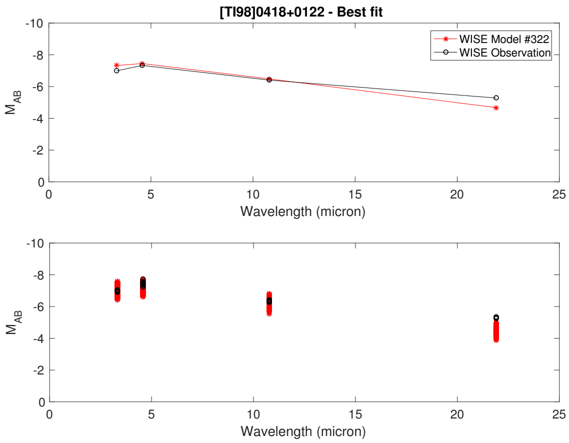

(a) **Object:** [TI98]0418+0122
Model: 322
T_{eff}: 2800 K
Mass: 1 $M_\odot$
logL: 4 $L_\odot$
C_{ex}: 8.8 log(C-O)+12
Class: wp
log$\dot{M}$: -5.7 $M_\odot$/year

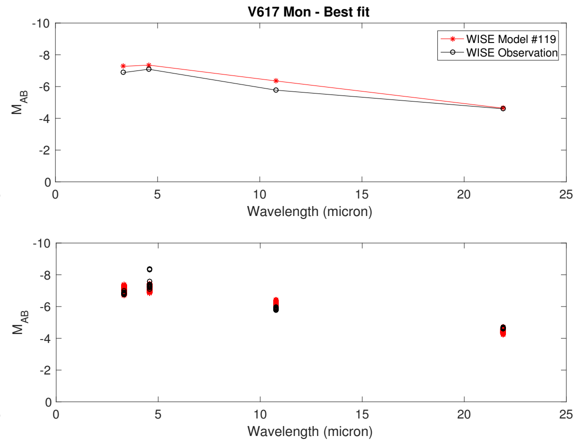

(b) **Object:** V617 Mon
Model: 119
T_{eff}: 2600 K
Mass: 1.5 $M_\odot$
logL: 4 $L_\odot$
C_{ex}: 8.5 log(C-O)+12
Class: wn
log$\dot{M}$: -5.14 $M_\odot$/year

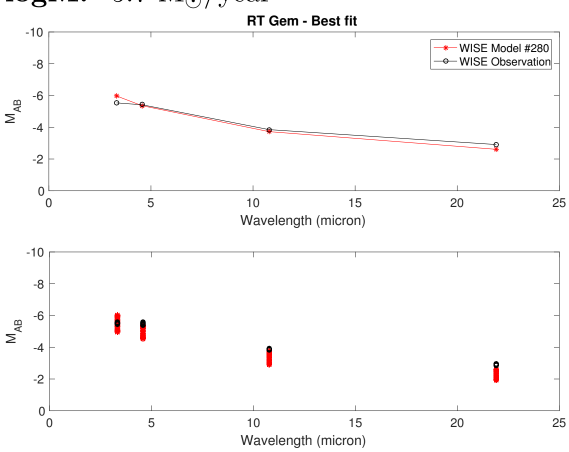

(c) **Object:** RT Gem
Model: 200
T_{eff}: 2800 K
Mass: 2 $M_\odot$
logL: 3.85 $L_\odot$
C_{ex}: 8.5 log(C-O)+12
Class: pp
log$\dot{M}$: N/A

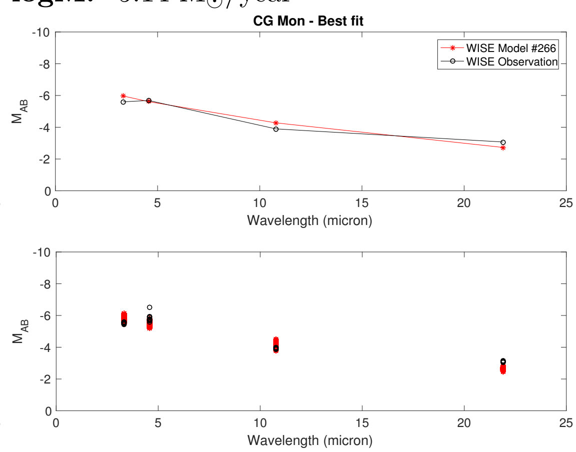

(d) **Object:** CG Mon
Model: 266
T_{eff}: 2800 K
Mass: 1 $M_\odot$
logL: 3.85 $L_\odot$
C_{ex}: 8.8 log(C-O)+12
Class: pp
log$\dot{M}$: N/A

Figure 4.2: Best fit and model info for object 1 – 4

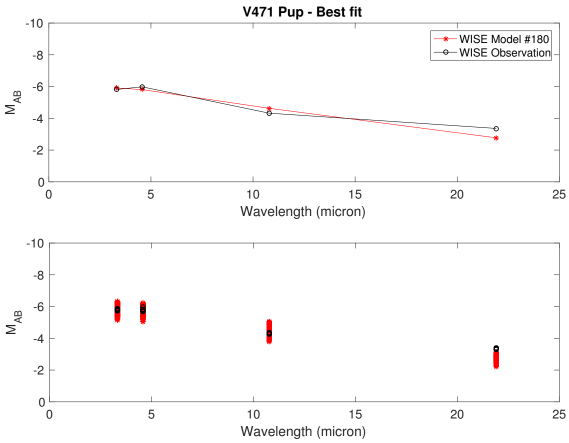

(a) **Object:** V471 Pup
Model: 100
$\mathbf{T_{eff}}$**:** 2800 K
Mass: 0.75 $M_\odot$
logL: 3.55 $L_\odot$
$\mathbf{C_{ex}}$**:** 8.8 log(C-O)+12
Class: wn
log$\dot{\mathbf{M}}$: -5.91 $M_\odot$/year

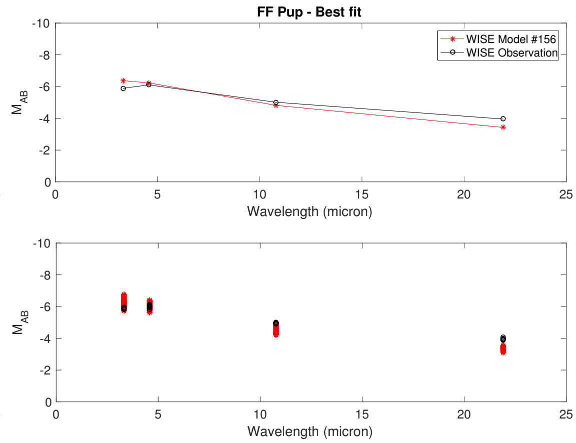

(b) **Object:** FF Pup
Model: 156
$\mathbf{T_{eff}}$**:** 2600 K
Mass: 2 $M_\odot$
logL: 4 $L_\odot$
$\mathbf{C_{ex}}$**:** 8.5 log(C-O)+12
Class: pm
log$\dot{\mathbf{M}}$: N/A

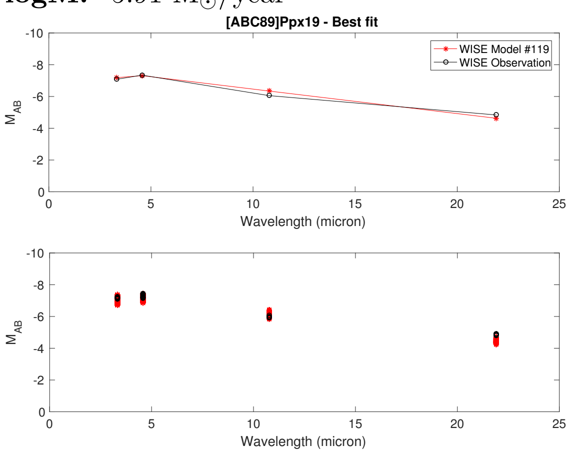

(c) **Object:** [ABC89]Ppx19
Model: 119
$\mathbf{T_{eff}}$**:** 2600 K
Mass: 1.5 $M_\odot$
logL: 4 $L_\odot$
$\mathbf{C_{ex}}$**:** 8.5 log(C-O)+12
Class: wn
log$\dot{\mathbf{M}}$: -5.14 $M_\odot$/year

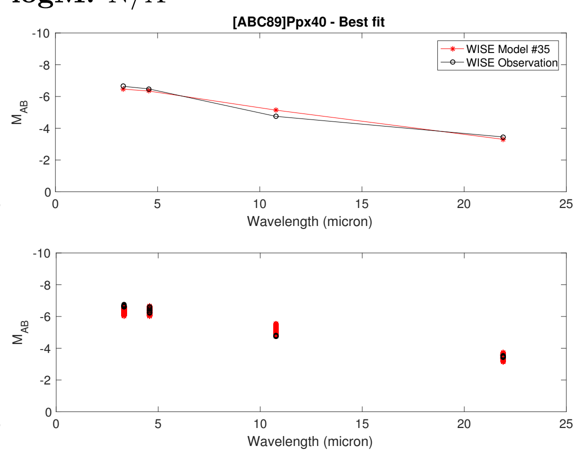

(d) **Object:** [ABC89]Ppx40
Model: 35
$\mathbf{T_{eff}}$**:** 2600 K
Mass: 1 $M_\odot$
logL: 3.7 $L_\odot$
$\mathbf{C_{ex}}$**:** 8.8 log(C-O)+12
Class: wn
log$\dot{\mathbf{M}}$: -5.54 $M_\odot$/year

Figure 4.3: Best fit and model info for object 5 – 8

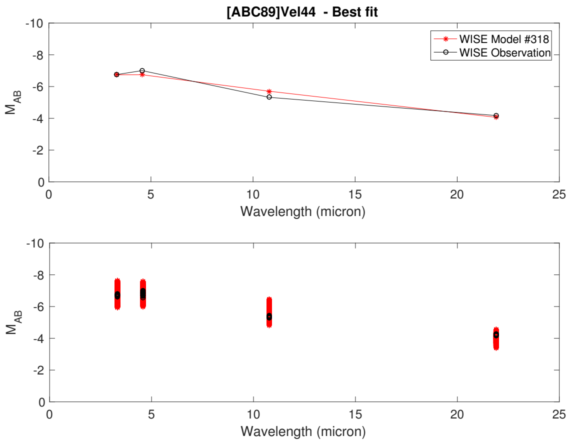

(a) **Object:** [ABC89]Vel44
Model: 318
$\mathbf{T_{eff}}$**:** 2800 K
Mass: 1 $M_\odot$
logL: 4 $L_\odot$
$\mathbf{C_{ex}}$**:** 8.5 log(C-O)+12
Class: wp
log$\dot{\mathbf{M}}$: -5.61 $M_\odot$/year

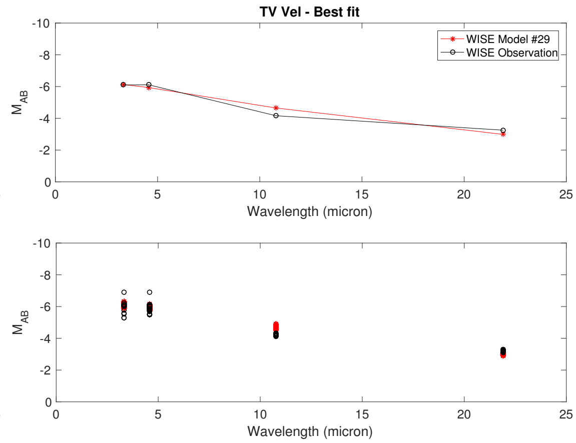

(b) **Object:** TV Vel
Model: 29
$\mathbf{T_{eff}}$**:** 2600 K
Mass: 1 $M_\odot$
logL: 3.7 $L_\odot$
$\mathbf{C_{ex}}$**:** 8.5 log(C-O)+12
Class: ws
log$\dot{\mathbf{M}}$: -5.8 $M_\odot$/year

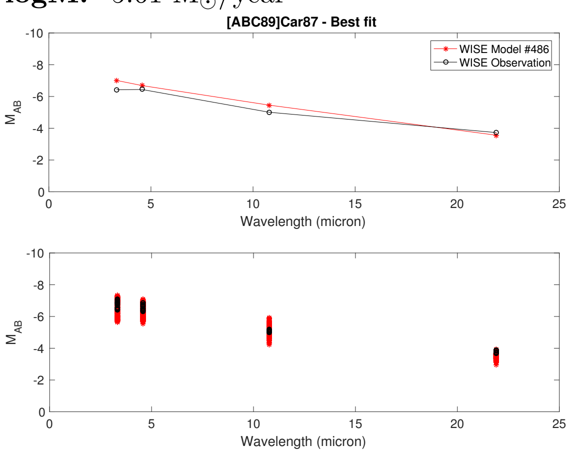

(c) **Object:** [ABC89]Car87
Model: 486
$\mathbf{T_{eff}}$**:** 3000 K
Mass: 1.5 $M_\odot$
logL: 4 $L_\odot$
$\mathbf{C_{ex}}$**:** 8.8 log(C-O)+12
Class: wn
log$\dot{\mathbf{M}}$: -5.78 $M_\odot$/year

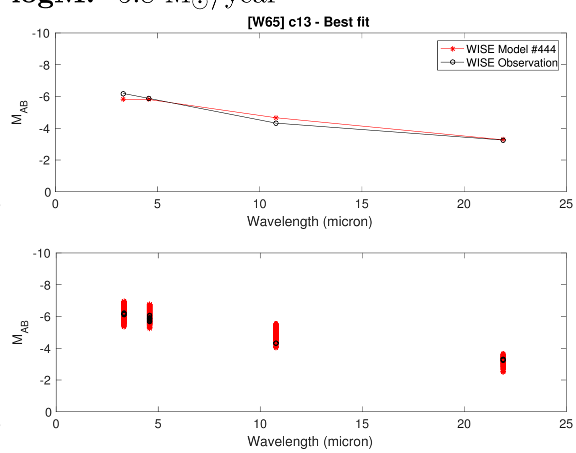

(d) **Object:** [W65] c13
Model: 444
$\mathbf{T_{eff}}$**:** 3000 K
Mass: 1 $M_\odot$
logL: 3.85 $L_\odot$
$\mathbf{C_{ex}}$**:** 8.5 log(C-O)+12
Class: pp
log$\dot{\mathbf{M}}$: N/A

Figure 4.4: Best fit and model info for object 9 – 12

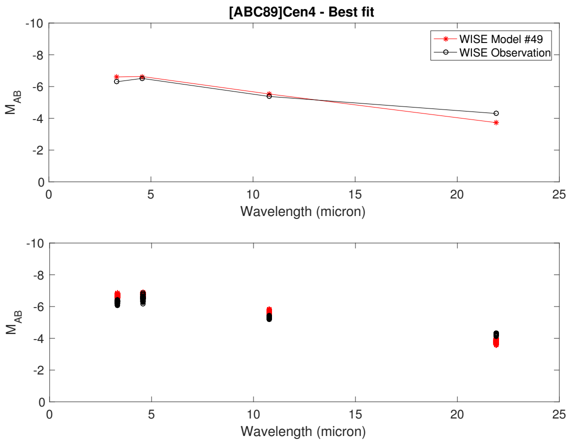

(a) **Object:** [ABC89]Cen4
Model: 49
T$_{\mathbf{eff}}$: 2600 K
Mass: 0.75 $M_\odot$
logL: 3.85 $L_\odot$
C$_{\mathbf{ex}}$: 8.8 log(C-O)+12
Class: wn
log$\dot{\mathbf{M}}$: -5.31 $M_\odot$/year

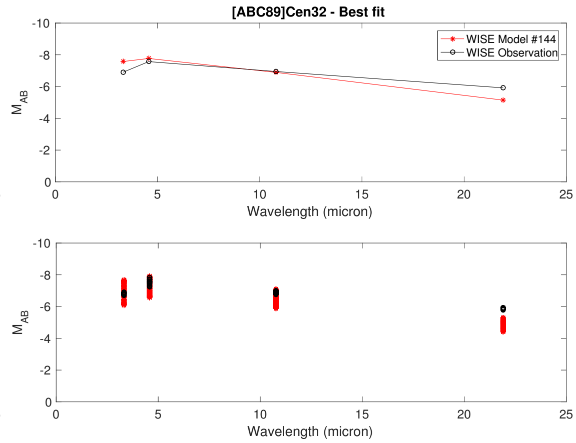

(b) **Object:** [ABC89]Cen32
Model: 144
T$_{\mathbf{eff}}$: 2600 K
Mass: 1 $M_\odot$
logL: 4 $L_\odot$
C$_{\mathbf{ex}}$: 8.8 log(C-O)+12
Class: wn
log$\dot{\mathbf{M}}$: -4.94 $M_\odot$/year

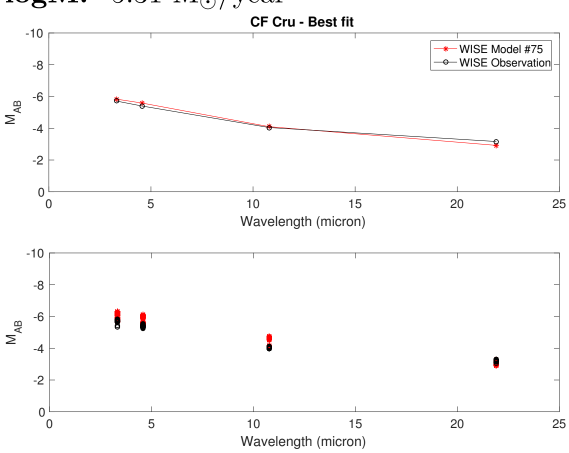

(c) **Object:** CF Cru
Model: 75
T$_{\mathbf{eff}}$: 2600 K
Mass: 1 $M_\odot$
logL: 3.85 $L_\odot$
C$_{\mathbf{ex}}$: 8.2 log(C-O)+12
Class: pp
log$\dot{\mathbf{M}}$: N/A

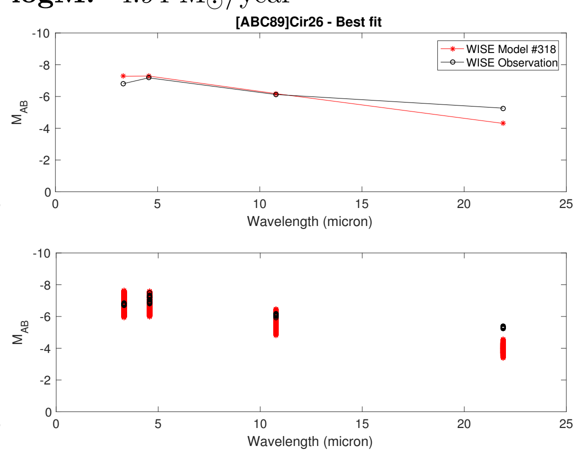

(d) **Object:** [ABC89]Cir26
Model: 318
T$_{\mathbf{eff}}$: 2800 K
Mass: 1 $M_\odot$
logL: 4 $L_\odot$
C$_{\mathbf{ex}}$: 8.5 log(C-O)+12
Class: wp
log$\dot{\mathbf{M}}$: -5.61 $M_\odot$/year

Figure 4.5: Best fit and model info for object 13 – 16

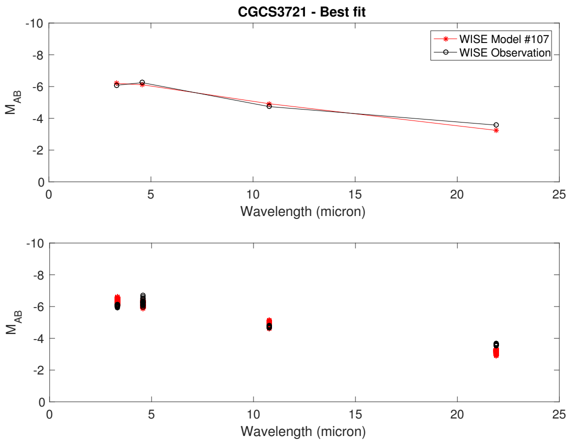

(a) **Object:** CGCS3721
Model: 107
$\mathbf{T_{eff}}$**:** 2600 K
Mass: 2 $M_{\odot}$
logL: 3.85 $L_{\odot}$
$\mathbf{C_{ex}}$**:** 8.8 log(C-O)+12
Class: wp
log$\dot{\mathbf{M}}$: -5.91 $M_{\odot}$/year

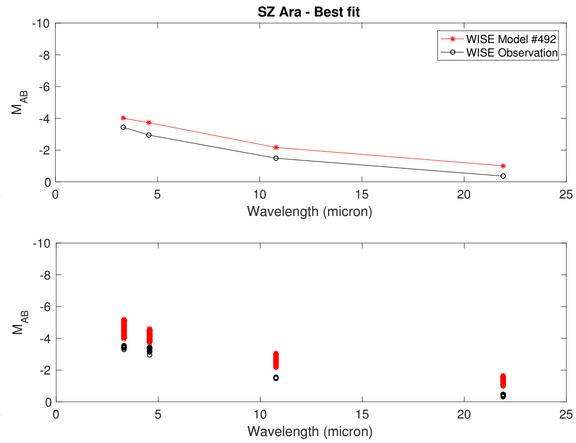

(b) **Object:** SZ Ara
Model: 492
$\mathbf{T_{eff}}$**:** 3200 K
Mass: 0.75 $M_{\odot}$
logL: 3.55 $L_{\odot}$
$\mathbf{C_{ex}}$**:** 8.2 log(C-O)+12
Class: pm
log$\dot{\mathbf{M}}$: N/A

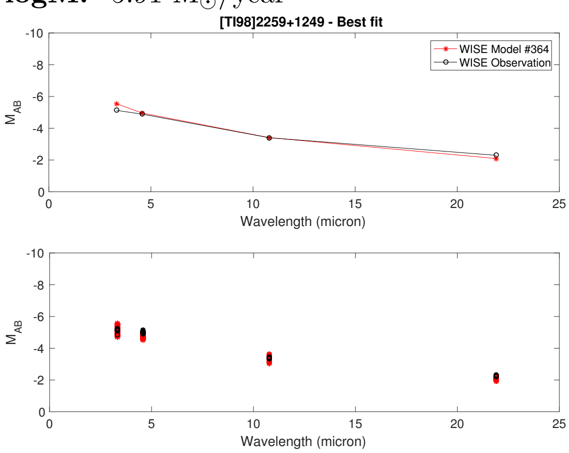

(c) **Object:** [TI98]2259+1249
Model: 364
$\mathbf{T_{eff}}$**:** 3000 K
Mass: 0.75 $M_{\odot}$
logL: 3.7 $L_{\odot}$
$\mathbf{C_{ex}}$**:** 8.2 log(C-O)+12
Class: pn
log$\dot{\mathbf{M}}$: N/A

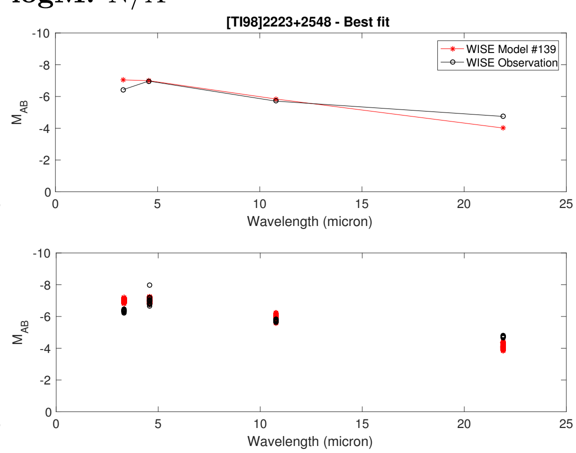

(d) **Object:** [TI98]2223+2548
Model: 139
$\mathbf{T_{eff}}$**:** 2600 K
Mass: 1 $M_{\odot}$
logL: 4 $L_{\odot}$
$\mathbf{C_{ex}}$**:** 8.8 log(C-O)+12
Class: wp
log$\dot{\mathbf{M}}$: -5.75 $M_{\odot}$/year

Figure 4.6: Best fit and model info for object 17 – 20

#	Object Name	$M_{W1\ obs}$	$M_{W1\ mod}$	$M_{W2\ obs}$	$M_{W2\ mod}$	$M_{W3\ obs}$	$M_{W3\ mod}$	$M_{W4\ obs}$	$M_{W4\ mod}$
1	[TI98]0418+0122	-6.9874	-7.3234	-7.3307	-7.4501	-6.4067	-6.4833	-5.2777	-4.6726
2	V617 Mon	-6.879	-7.2711	-7.0917	-7.3525	-5.7747	-6.3541	-4.5997	-4.6359
3	RT Gem	-5.5341	-5.971	-5.4155	-5.3578	-3.8505	-3.7238	-2.9105	-2.6099
4	CG Mon	-5.6013	-5.9689	-5.6863	-5.612	-3.8973	-4.2771	-3.0713	-2.727
5	V471 Pup	-5.8175	-5.9132	-5.9857	-5.8105	-4.3247	-4.6315	-3.3627	-2.7714
6	FF Pup	-5.8907	-6.3729	-6.1047	-6.2375	-5.0137	-4.8187	-3.9547	-3.4279
7	[ABC89]Ppx19	-7.082	-7.1854	-7.3446	-7.3136	-6.0546	-6.3423	-4.8366	-4.6272
8	[ABC89]Ppx40	-6.6409	-6.4629	-6.4796	-6.3433	-4.7496	-5.1404	-3.4506	-3.3
9	[ABC89]Vel44	-6.7528	-6.74	-7.0049	-6.7444	-5.3219	-5.7072	-4.1739	-4.0617
10	TV Vel	-6.0994	-6.1277	-6.1111	-5.9373	-4.1641	-4.6519	-3.2531	-2.9861
11	[ABC89]Car87	-6.4242	-7.0116	-6.4402	-6.6877	-5.0082	-5.4557	-3.7272	-3.5609
12	[W65] c13	-6.1926	-5.817	-5.8829	-5.8123	-4.3229	-4.6624	-3.2549	-3.2725
13	[ABC89]Cen4	-6.3008	-6.6059	-6.5133	-6.6341	-5.3773	-5.5313	-4.3033	-3.7275
14	[ABC89]Cen32	-6.9036	-7.5778	-7.5723	-7.77	-6.9493	-6.8928	-5.9183	-5.1447
15	CF Cru	-5.711	-5.8328	-5.3999	-5.5871	-4.0449	-4.0996	-3.1649	-2.9213
16	[ABC89]Cir26	-6.8067	-7.2761	-7.1746	-7.2885	-6.1246	-6.1815	-5.2656	-4.3024
17	CGCS3721	-6.0805	-6.1984	-6.2468	-6.115	-4.7388	-4.9209	-3.5718	-3.2406
18	SZ Ara	-3.4389	-4.0048	-2.9479	-3.729	-1.4889	-2.1659	-0.3599	-1.0099
19	[TI98]2259+1249	-5.126	-5.5427	-4.8892	-4.9587	-3.4042	-3.4112	-2.2952	-2.091
20	[TI98]2223+2548	-6.43	-7.0444	-6.9706	-6.9975	-5.7076	-5.8417	-4.7436	-4.0119

Table 4.2: List of the observed (obs) and the model (mod) magnitudes in the different WISE bands. All magnitudes are in absolute AB magnitudes. The average deviation (object 18 is not included in the average deviation calculation) is 4.87 % in W1, 2.12 % in W2, 4.75 % in W3 and 10.53 % in W4.

Chapter 5

Discussion & Outlook

The fits seems to agree very well with the observations. The anomaly here is object number 18: SZ Ara. Here the fit displays a clearly visible offset from the observations as can be seen in Figure 4.6b. The fit deviates 14.13 % in W1, 20.95 % in W2, 31.26 % in W3 and 64.36 % in W4. This could be due to an incorrect distance given in Whitelock et al. (2006) where the distance for SZ Ara is given as 2.44 kpc. Creating a MATLAB script that calculated the distance that gave the best fit with the model we found the optimal distance to be 1.74 kpc. The new fit can be seen in Figure 5.1 below.

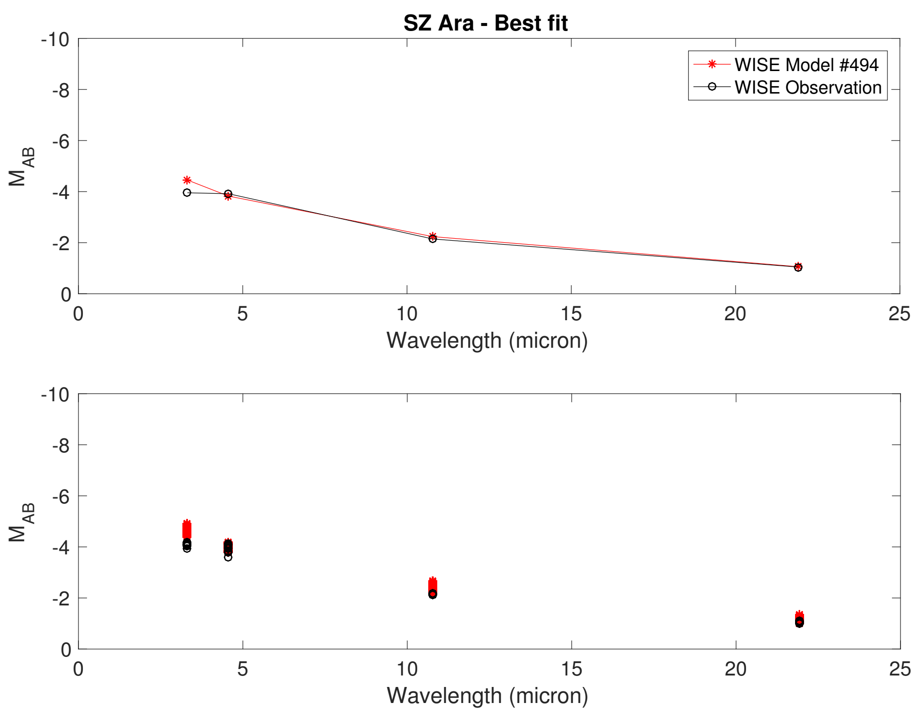

Figure 5.1: SZ Ara refitted with its distance set to 1.74 kpc. The fit now deviates 2.14 % in W1, 3.47 % in W2, 1.17 % in W3 and 0.17 % in W4.

Because of the saturation of most objects in WISE the stars that could be matched are very faint and currently not very well studied. It is therefore not possible to check what model parameters that match the observations except for mass loss that have been determined only for four objects in Whitelock et al. (2006). The mass loss however seems to agree fairly well with observations. Although the fits appears to be good one should not read too much into this since WISE only provides data for four filters. In this study we have only presented the best fitted model to each observation. There are however other models with slightly different parameters that also fit the observations good. Until more data is available on the stars it is hard to say if these other models might provide a better representation.

A logical next step in the wait for data from JWST would be to use data from another infrared telescope like the Spitzer Space Telescope or Herschel Space Observatory. One could also look at how spectroscopic data compares to the matched model spectra.

It should be a fairly simple task to incorporate more models in our dataset in the future as newer and more advanced model become available. In this study we have focused on C-stars but grids covering other types of AGB stars could of course also be incorporated, for example the M-star grid in Bladh et al. (2013).

Chapter 6

Conclusion

We have performed synthetic photometry for several filter systems using theoretical spectra and shown that it is possible to fit the resulting SEDs to observations with good results. We hope that future users of JWST will find our predictions useful and will help them to plan their observing strategies.

The photometric data set can be accessed at http://www.astro.uu.se/AGBmodels/

Acknowledgement

I would first like to thank my supervisor Erik Zackrisson who throughout this work have provided excellent guidance and also giving me the opportunity to attend the conference Cool Stars 19 and show this work to a bigger audience than otherwise possible. I would also like to thank my family for their support. A special thanks also to Kjell Eriksson for all his help when I had trouble with the spectral data.

Bibliography

Arianespace - ESA - NASA. Jwst launch configuration, 2009. URL `http://sci.esa.int/jwst/45742-jwst-launch-configuration/`.

S. Bladh, S. Höfner, W. Nowotny, B. Aringer, and K. Eriksson. Exploring wind-driving dust species in cool luminous giants. *A&A*, 553:A20, 2013. doi: 10.1051/0004-6361/201220590. URL `http://dx.doi.org/10.1051/0004-6361/201220590`.

J. A. Cardelli, G. C. Clayton, and J. S. Mathis. The relationship between infrared, optical, and ultraviolet extinction. *ApJ*, 345:245–256, Oct. 1989. doi: 10.1086/167900.

B. W. Carroll and D. A. Ostlie. *An Introduction to Modern Astrophysics*, chapter 13. Pearson Education Limited, second edition, 2014.

Doug Welch. Doug's excellent absorption law calculator. URL `http://dogwood.physics.mcmaster.ca/Acurve.html`.

Eriksson, K., Nowotny, W., Höfner, S., Aringer, B., and Wachter, A. Synthetic photometry for carbon-rich giants. *A&A*, 566:A95, 2014. doi: 10.1051/0004-6361/201323241. URL `http://dx.doi.org/10.1051/0004-6361/201323241`.

ESA/Hubble. Large and small stars in harmonious coexistence, 2006. URL `http://www.spacetelescope.org/images/heic0607a/`.

ESO. Hertzsprung-russell diagram, 2007. URL `https://www.eso.org/public/images/eso0728c/`.

A. Hjort and M. Holmberg. Photo of m27, 2015.

S. Höfner, S. Bladh, B. Aringer, and R. Ahuja. Dynamic atmospheres and winds of cool luminous giants, I. Al_2O_3 and silicate dust in the close vicinity of M-type AGB stars. *ArXiv e-prints*, May 2016.

IPAC/Caltech. Wise data processing, 2012. URL `http://wise2.ipac.caltech.edu/docs/release/allsky/expsup/sec4_4h.html`.

M. Meixner. Space observatory studies of agb stars in galaxies: from iras to jwst. *ASP Conference Series*, 445, 2011.

NASA/STScI. James webb space telescope nircam, 2016a. URL http://jwst.nasa.gov.

NASA/STScI. James webb space telescope miri, 2016b. URL http://www.stsci.edu/jwst/instruments/miri/.

NASA/STScI. James webb space telescope, 2016c. URL http://www.stsci.edu/jwst/instruments/nircam/.

NOAO/AURA/NSF. Asymptotic giant branch (agb) stars, 2003. URL https://www.noao.edu/outreach/press/pr03/sb0307.html.

Northrop Grumman. James webb space telescope (jwst). URL http://www.northropgrumman.com/MediaResources/Pages/Photo.aspx?pid%3DJW-12013_005%26rel%3D%2F%26name%3DPhotos.

D. Prialnik. *An Introduction to the Theory of Stellar Structure and Evolution*, chapter 4 & 9. Cambridge University Press, second edition, 2009.

Spanish Virtual Observatory. Filter profile service, 2012. URL http://svo2.cab.inta-csic.es/svo/theory/fps3/index.php?mode=browse.

P. A. Whitelock, M. W. Feast, F. Marang, and M. A. T. Groenewegen. Near-infrared photometry of carbon stars. *Monthly Notices of the Royal Astronomical Society*, 369(2): 751–782, 2006. ISSN 1365-2966. doi: 10.1111/j.1365-2966.2006.10322.x. URL http://dx.doi.org/10.1111/j.1365-2966.2006.10322.x.

Wikimedia Commons. Cno cycle, 2006. URL hhttps://commons.wikimedia.org/wiki/File:CNO_Cycle.svg.

This publication makes use of data products from the Wide-field Infrared Survey Explorer, which is a joint project of the University of California, Los Angeles, and the Jet Propulsion Laboratory/California Institute of Technology, funded by the National Aeronautics and Space Administration.

Appendix A

Filter systems

A.1 NIRCam

Filter	F070W	F090W	F115W	F150W	F200W	F277W	F356W	F444W
λ_{eff}	0.70	0.90	1.15	1.50	2.00	2.77	3.56	4.44

Table A.1: NIRCam filters used and the corresponding λ_{eff} (NASA/STScI, 2016c)

A.2 MIRI

Filter	F560W	F770W	F1000W	F1130W	F1280W	F1500W	F1800W	F2100W
λ_{eff}	5.60	7.70	10.00	11.30	12.80	15.00	18.00	21.00

Table A.2: MIRI filters used and the corresponding λ_{eff} (NASA/STScI, 2016b)

A.3 WISE

Filter	W1	W2	W3	W4
λ_{eff}	3.3157	4.5645	10.7868	21.9150

Table A.3: WISE filters used and the corresponding λ_{eff} (Spanish Virtual Observatory, 2012)

A.4 Generic

Filter	UX	BX	B	V	R	I	J	J2m
λ_{eff}	0.366	0.438	0.438	0.545	0.641	0.798	1.220	1.235
Filter	H	H2m	Ks2m	K	L	Lp	M	Mp
λ_{eff}	1.630	1.662	2.159	2.19	3.45	3.80	4.75	4.80

Table A.4: Generic filters (filters ending in 2m is from 2MASS(Spanish Virtual Observatory, 2012)) used in Eriksson, K. et al. (2014) and the corresponding λ_{eff}

Appendix B

Grid parameters

T_* [K]	$\log L_*$ [$L_\odot$]	P [days]	M_* [$M_\odot$]	$\log$ (C-O) + 12 [dex]
2600	3.70	294	0.75, 1.0	8.2, 8.5, 8.8
	3.85	390	0.75, 1.0, 1.5, 2.0	8.2, 8.5, 8.8
	4.0	525	1.0, 1.5, 2.0	8.2, 8.5, 8.8
2800	3.55	221	0.75	8.2, 8.5, 8.8
	3.70	294	0.75, 1.0	8.2, 8.5, 8.8
	3.85	390	0.75, 1.0, 1.5, 2.0	8.2, 8.5, 8.8
	4.00	525	1.0, 1.5, 2.0	8.2, 8.5, 8.8
3000	3.55	221	0.75	8.2, 8.5, 8.8
	3.70	294	0.75, 1.0	8.2, 8.5, 8.8
	3.85	390	0.75, 1.0, 1.5, 2.0	8.2, 8.5, 8.8
	4.00	525	1.5	8.2, 8.5, 8.8
3200	3.55	221	0.75	8.2, 8.5, 8.8
	3.79	294	0.75, 1.0	8.2, 8.5, 8.8

Table B.1: Stellar parameters used in the the grid by Eriksson, K. et al. (2014)

Class		**Description**
pp	=	Pulsating atmosphere, periodically pulsating models, repeating their dynamic behaviour every period.
pm	=	Pulsating atmosphere, multi-periodic models, models that repeat after two (sometimes more) periods.
pn	=	Pulsating atmosphere, irregular models (non-periodic).
ws	=	Wind, models with a steady wind with small temporal variations in mass-loss rates and wind velocities.
wp	=	Wind, periodic variations in the wind properties.
wn	=	Wind, models with more irregular behaviour (non-periodic).
we	=	Wind, episodic models, that show an intermittent outflow.

Table B.2: Explanation for different model classes used in Eriksson, K. et al. (2014)

Appendix C

Code

On the following pages a selection of the codes used throughout this study is presented. In order for the code to function properly the photometric data from this study and the spectra from Eriksson, K. et al. (2014) need to be present in the same folders as the code. Several other codes that are necessary for the programs to work where also developed but they are not presented below, they are however available together with the online data in the correct folder structure at http://www.astro.uu.se/AGBmodels/.

C.1 Process spectra

C.1.1 main.m

```
%% Main file for calculating the photometric flux from synthetic spectra
% Adam Hjort 2016
%% Import constants and data
tic;
constants
import_data;      % Import data on spectra located in data/spectra.dat
import_tabelb1
%% Select model to work with and filter system
l = 0;          % Select model, if 0 a range of models will be used
l_range = 1:Mod(end);   % Select range of models. l must be 0

filter_system = 'JWST'; % Select JWST, NIRCam, MIRI, WISE or generic
[filter_list, filter_data] = filter_config(filter_system);

%% Select output
plot_results = 1;   % 1 for making plots, 0 skips this.
plot_save = 0; % 1 for saving plots, 0 skips this. plot_result must be = 1
inputoutput_format_master
if l == 0

    %% Multiple models
```

```
    for l = l_range
        modsrc = char(strcat('data/DMAspectra/', SpFolderName(l)));
        mod_src = dir(modsrc);
        n = 1;
        for m = 1:length(mod_src)
            if mod_src(m).isdir == 1 & mod_src(m).name~='.'
                folders(:,n) = {mod_src(m).name};
                n = n+1;
            end
        end

        for o = 1:length(folders)
            import_modinfo
            inputoutput_format_epoch
            for p = 1:length(spectra_name)
                input_output_single
                process_spectrum
                save_data
                plot_data
            end
        end
        clear folders
    end
else
%% Single model
    modsrc = char(strcat('data/DMAspectra/', SpFolderName(l)));
    mod_src = dir(modsrc);
    n = 1;
    for m = 1:length(mod_src)
        if mod_src(m).isdir == 1 & mod_src(m).name~='.'
            folders(:,n) = {mod_src(m).name};
            n = n+1;
        end
    end

    for o = 1:length(folders)
        import_modinfo
        inputoutput_format_epoch
        for p = 1:length(spectra_name)
            input_output_single
            process_spectrum
            save_data
            plot_data
        end
    end
end
disp('FINISHED!')
toc;
```

C.1.2 process_spectrum.m

```
%% processSpectrum.m.m
%  Adam Hjort 2016 based on code by Erik Zackrisson
%  Load spectrum in format: (Wavelength in Angstrom (A), Flux in erg/s)
%---------------------------------
raw_spec=load(infile_spec);
wave_spec=raw_spec(:,1)'; % Angstrom
flux_spec_flambda(1,:)=raw_spec(:,3)'; % erg/s
flux_spec_flambda = flux_spec_flambda./wave_spec; % convert to erg/s/A
spectra=1;
ind=size(wave_spec,2);
disp(['Processing model: ' num2str(Mod(l))])
disp(['Processing epoch: ' num2str(o)])
disp(['Processing spectra: ' num2str(p)])

% For all filter profiles listed in the file list
% -------------------------------------
names_mod=char(textread(filter_list,'%q'));
for filter=1:(size(names_mod,1))
    current_filter=names_mod(filter,:); % Extract name of current model
    while (current_filter(size(current_filter,2))==' ')
        current_filter=current_filter(1:(size(current_filter,2)-1));
    end

    % Load transmission curve
    % -----------------------
    raw_trans=load([filter_data '/' current_filter]);
    wave_trans=raw_trans(:,1); % Angstrom
    trans=raw_trans(:,2);

    % For every redshift
    % ------------------
    for j=1:size(z_range,2)

        z=z_range(j);

        % Correct spectrum for redshift
        % -----------------------------
        wave_spec_z=wave_spec.*(1+z);
        flux_spec_flambda_z=flux_spec_flambda./(1+z);


        % Absorption shortward of (and possibly including) Lya
        % ---------------------------------------------------
        if (Lyalphaabs_alt==2 && z>z_reion)
            ind_abs=find(wave_spec_z < 1220.*(1+z));
            flux_spec_flambda_z(ind_abs)=0;
        end
        if (Lyalphaabs_alt==3 && z>z_reion)
```

```
            ind_abs=find(wave_spec_z < 1210.*(1+z));
            flux_spec_flambda_z(ind_abs)=0;
        end

        % Convert spectrum and transmission curve to fnu & nu
        % -----------------------------------------------------
        freq_spec_z = zeros(1,length(raw_spec));
         for k=1:spectra
             freq_spec_z(k,1:ind(k))=c./(wave_spec_z...
                 (k,1:ind(k)).*1e-10); % Hz
         end

        freq_trans=c./(wave_trans.*1e-10); % Hz

        flux_spec_fnu_z = zeros(1,length(raw_spec));
        for k=1:spectra
            flux_spec_fnu_z(k,1:ind(k))=flux_spec_flambda_z...
                (k,1:ind(k)).*1e10.*(wave_spec_z...
                (k,1:ind(k)).*1e-10).^2./c; % erg s^-1 Hz^-1
            flux_spec_fnu_z(k,1:ind(k))=flux_spec_fnu_z(k,1:ind(k))./...
                (4.*pi.*(10.*pc.*100).^2); % erg/s^-1/cm^-2/Hz^-1
        end


        % Interpol. spectrum and trans curve to common frequency scale
        % ------------------------------------------------------------------
        freq_trans_min=min(freq_trans);
        freq_trans_max=max(freq_trans);
        delta_freq=(freq_trans_max-freq_trans_min)./(Nint-1);
        freq_trans_int=freq_trans_min:delta_freq:freq_trans_max;

        trans_int=interp1(freq_trans,trans,freq_trans_int);
        flux_spec_fnu_z_int = zeros(1,Nint);
        for k=1:spectra
            flux_spec_fnu_z_int(k,:)=interp1(freq_spec_z(k,1:ind(k)),...
                flux_spec_fnu_z(k,1:ind(k)),freq_trans_int);
            ind_nan=find(isnan(flux_spec_fnu_z_int(k,:))==1);
            flux_spec_fnu_z_int(k,ind_nan)=0;
        end

        % Compute absolute AB magnitude
        % ------------------------------
        Sum_Tnu_dnu=sum(trans_int).*delta_freq;
        for k=1:spectra
            Sum_Fnu_Tnu_dnu(k)=...
                sum(flux_spec_fnu_z_int(k,:).*trans_int).*delta_freq;
            M_AB(k,filter,j)=-2.5.*log10(Sum_Fnu_Tnu_dnu(k)./...
                Sum_Tnu_dnu)-48.60; % M_AB(timestep,filter,z)
        end

        % End loop over all redshifts
```

```
        % ---------------------------
    end

    % End loop over all filters
    % -------------------------
end

% Derive luminosity distance
% --------------------------
d_L = zeros(1,size(z_range,2));
for j=1:size(z_range,2)
    d_L(j)=(1+z_range(j)).*1e-3.*c./H0.*quadl('distfunc',0,z_range(j)...
        ,[],[],Omega_M,Omega_Lambda); % Mpc
end

% Derive apparent magnitude
% -------------------------
for j=1:size(z_range,2)
    if (z_range(j)==0)
        m_AB(:,:,j)=M_AB(:,:,j); % m_AB(timestep,filter,z)
    end
    if (z_range(j)~=0)
        if (mag_opt==1)
            m_AB(:,:,j)=5.*log10(d_L(j))+25+M_AB(:,:,j);
            % m_AB(timestep,filter,z)
        end
        if (mag_opt==2)
            m_AB(:,:,j)=M_AB(:,:,j);
        end
    end

end
```

C.1.3 save_data.m

```
%% Write data to .dat files
% Adam Hjort 2016

% Spectrum - FILTERS - Phase Teff Mass logL Cex Dup fL Model logg Epoch
epoch_extra_start = spectra_name(p);
epoch_format_start = '%5.0f\t ';
epoch_extra_end = [phase(p) Teff(l) Mass(l) logL(l) Cex(l) Dup(l) ...
    fL(l) Mod(l) logg(l) str2double(char(folders(o)))];
epoch_format_end = [' %5f\t %5.0f\t %5.3f\t %5.3f\t %5.3f\t '...
    '%5.3f\t %5.3f\t %5.0f\t %5.3f\t %5.0f\n'];

% Model Epoch Spectrum - FILTERS - Phase Epoch_cur Epoch_tot Teff Mass
% logL Cex Dup fL logg
master_extra_start = [Mod(l) str2double(char(folders(o))) spectra_name(p)];
master_format_start = '%5.0f\t %5.0f\t %5.0f\t ';
```

```
master_extra_end = [phase(p) o length(folders) Teff(l) Mass(l) logL(l) ...
    Cex(l) Dup(l) fL(l) logg(l)];
master_format_end = [' %5f\t %5.0f\t %5.0f\t %5.0f\t %5.3f\t '...
    '%5.3f\t %5.3f\t %5.3f\t %5.3f\t %5.3f\n'];
% Write results to output file

switch filter_system
    case 'JWST'
        %% JWST
        m_F070W=m_AB(:,1,:);
        m_F115W=m_AB(:,2,:);
        m_F150W=m_AB(:,3,:);
        m_F200W=m_AB(:,4,:);
        m_F277W=m_AB(:,5,:);
        m_F356W=m_AB(:,6,:);
        m_F444W=m_AB(:,7,:);
        m_F560W=m_AB(:,8,:);
        m_F770W=m_AB(:,9,:);
        m_F1000W=m_AB(:,10,:);
        m_F1130W=m_AB(:,11,:);
        m_F1280W=m_AB(:,12,:);
        m_F1500W=m_AB(:,13,:);
        m_F1800W=m_AB(:,14,:);
        m_F2100W=m_AB(:,15,:);
        m_F2550W=m_AB(:,16,:);
        m_F090W=m_AB(:,17,:);


        ind_nan=find(isnan(m_AB)==1);
        ind_inf=find(isinf(m_AB)==1);
        m_AB(ind_nan)=999.0;
        m_AB(ind_inf)=999.0;

        % ----------------------------
        % NIRCam: F070W F090W F115W F150W F200W F277W F356W F444W
        fid1=fopen([outdir '/' epoch_name '_JWST_NIRCam_ABmag.dat'],'a');
        fprintf(fid1,[epoch_format_start '%9.4f\t %9.4f\t %9.4f\t' ...
            ' %9.4f\t %9.4f\t %9.4f\t %9.4f\t %9.4f\t' epoch_format_end]...
            ,[epoch_extra_start m_AB(1,1) m_AB(1,17) m_AB(1,2) m_AB(1,3) ...
            m_AB(1,4) m_AB(1,5) m_AB(1,6) m_AB(1,7) epoch_extra_end]);
        fclose(fid1);
        % MIRI: F560W F770W F1000W F1130W F1280W m_F1500W F1800W F2100W
        % Note that F2550W is intentionally not included
        fid2=fopen([outdir '/' epoch_name '_JWST_MIRI_ABmag.dat'],'a');
        fprintf(fid2,[epoch_format_start '%9.4f\t %9.4f\t %9.4f\t '...
            '%9.4f\t %9.4f\t %9.4f\t %9.4f\t %9.4f\t' epoch_format_end],...
            [epoch_extra_start m_AB(1,8) m_AB(1,9) m_AB(1,10) m_AB(1,11)...
            m_AB(1,12) m_AB(1,13) m_AB(1,14) m_AB(1,15) epoch_extra_end]);
        fclose(fid2);

        if multi_spectra == 1
```

```
            fid3=fopen([outdir '/JWST_NIRCam_ABmag.dat'],'a');
            fprintf(fid3,[master_format_start '%9.4f\t %9.4f\t %9.4f\t '...
                '%9.4f\t %9.4f\t %9.4f\t %9.4f\t %9.4f\t' ...
                master_format_end], [master_extra_start m_AB(1,1)...
                m_AB(1,17) m_AB(1,2) m_AB(1,3) m_AB(1,4) m_AB(1,5)...
                m_AB(1,6) m_AB(1,7) master_extra_end]);
            fclose(fid3);

            fid4=fopen([outdir '/JWST_MIRI_ABmag.dat'],'a');
            fprintf(fid4,[master_format_start '%9.4f\t %9.4f\t %9.4f\t '...
                '%9.4f\t %9.4f\t %9.4f\t %9.4f\t %9.4f\t'...
                master_format_end], [master_extra_start m_AB(1,8) ...
                m_AB(1,9) m_AB(1,10) m_AB(1,11) m_AB(1,12) m_AB(1,13) ...
                m_AB(1,14) m_AB(1,15) master_extra_end]);
            fclose(fid4);
        end
    case 'NIRCam'
        %% NIRCam
        %  NIRCam: F070W F090W F115W F150W F200W F277W F356W F444W
        m_F070W=m_AB(:,1,:);
        m_F115W=m_AB(:,2,:);
        m_F150W=m_AB(:,3,:);
        m_F200W=m_AB(:,4,:);
        m_F277W=m_AB(:,5,:);
        m_F356W=m_AB(:,6,:);
        m_F444W=m_AB(:,7,:);
        m_F090W=m_AB(:,8,:);

        ind_nan=find(isnan(m_AB)==1);
        ind_inf=find(isinf(m_AB)==1);
        m_AB(ind_nan)=999.0;
        m_AB(ind_inf)=999.0;

        % Write results to output file
        % ----------------------------
        fid1=fopen([outdir '/' epoch_name '_JWST_NIRCam_ABmag.dat'],'a');
        fprintf(fid1,[epoch_format_start '%9.4f\t %9.4f\t %9.4f\t '...
            '%9.4f\t %9.4f\t %9.4f\t %9.4f\t %9.4f\t' epoch_format_end],...
            [epoch_extra_start m_AB(1,1) m_AB(1,8) m_AB(1,2) m_AB(1,3) ...
            m_AB(1,4) m_AB(1,5) m_AB(1,6) m_AB(1,7) epoch_extra_end]);
        fclose(fid1);

        if multi_spectra == 1
            fid2=fopen([outdir '/JWST_NIRCam_ABmag.dat'],'a');
            fprintf(fid2,[master_format_start '%9.4f\t %9.4f\t %9.4f\t '...
                '%9.4f\t %9.4f\t %9.4f\t %9.4f\t %9.4f\t' ...
                master_format_end], [master_extra_start m_AB(1,1) ...
                m_AB(1,8) m_AB(1,2) m_AB(1,3) m_AB(1,4) m_AB(1,5) ...
                m_AB(1,6) m_AB(1,7) master_extra_end]);
            fclose(fid2);
        end
```

```
    case 'MIRI'
        %% MIRI
        %  MIRI: F560W F770W F1000W F1130W F1280W m_F1500W F1800W F2100W
        %  Note that F2550W is intentionally not included
        m_F560W=m_AB(:,1,:);
        m_F770W=m_AB(:,2,:);
        m_F1000W=m_AB(:,3,:);
        m_F1130W=m_AB(:,4,:);
        m_F1280W=m_AB(:,5,:);
        m_F1500W=m_AB(:,6,:);
        m_F1800W=m_AB(:,7,:);
        m_F2100W=m_AB(:,8,:);
        m_F2550W=m_AB(:,9,:);


        ind_nan=find(isnan(m_AB)==1);
        ind_inf=find(isinf(m_AB)==1);
        m_AB(ind_nan)=999.0;
        m_AB(ind_inf)=999.0;

        % Write results to output file
        % ----------------------------
        fid1=fopen([outdir '/' epoch_name '_JWST_MIRI_ABmag.dat'],'a');
        fprintf(fid1,[epoch_format_start '%9.4f\t %9.4f\t %9.4f\t '...
            '%9.4f\t %9.4f\t %9.4f\t %9.4f\t %9.4f\t %9.4f\t' ...
            epoch_format_end], [epoch_extra_start m_AB(1,1) m_AB(1,2) ...
            m_AB(1,3) m_AB(1,4) m_AB(1,5) m_AB(1,6) m_AB(1,7) m_AB(1,8) ...
            m_AB(1,9) epoch_extra_end]);
        fclose(fid1);
        if multi_spectra == 1
            fid2=fopen([outdir '/JWST_MIRI_ABmag.dat'],'a');
            fprintf(fid2,[master_format_start '%9.4f\t %9.4f\t %9.4f\t '...
                '%9.4f\t %9.4f\t %9.4f\t %9.4f\t %9.4f\t %9.4f\t' ...
                master_format_end], [master_extra_start m_AB(1,1) ...
                m_AB(1,2) m_AB(1,3) m_AB(1,4) m_AB(1,5) m_AB(1,6) ...
                m_AB(1,7) m_AB(1,8) m_AB(1,9) master_extra_end]);
            fclose(fid2);
        end
    case 'WISE'
        %% WISE
        %  W1 W2 W3 W4
        W1=m_AB(:,1,:);
        W2=m_AB(:,2,:);
        W3=m_AB(:,3,:);
        W4=m_AB(:,4,:);


        ind_nan=find(isnan(m_AB)==1);
        ind_inf=find(isinf(m_AB)==1);
        m_AB(ind_nan)=999.0;
        m_AB(ind_inf)=999.0;
```

```
        % Write results to output file
        % ----------------------------
        fid1=fopen([outdir '/' epoch_name '_WISE_ABmag.dat'],'a');
        fprintf(fid1,[epoch_format_start ...
            '%9.4f\t %9.4f\t %9.4f\t %9.4f\t' epoch_format_end],...
            [epoch_extra_start m_AB(1,1) m_AB(1,2) m_AB(1,3) m_AB(1,4) ...
               epoch_extra_end]);
        fclose(fid1);
        if multi_spectra == 1
            fid2=fopen([outdir '/WISE_ABmag.dat'],'a');
            fprintf(fid2,[master_format_start ...
                '%9.4f\t %9.4f\t %9.4f\t %9.4f\t' master_format_end],...
                [master_extra_start m_AB(1,1) m_AB(1,2) m_AB(1,3) ...
                m_AB(1,4) master_extra_end]);
            fclose(fid2);
        end
    case 'generic'
        %% Generic
        %  UX BX B V R I J J2m H H2m Ks2m K L Lp M Mp
        UX=m_AB(:,1,:);
        BX=m_AB(:,2,:);
        B=m_AB(:,3,:);
        V=m_AB(:,4,:);
        R=m_AB(:,5,:);
        I=m_AB(:,6,:);
        J=m_AB(:,7,:);
        H=m_AB(:,8,:);
        K=m_AB(:,9,:);
        L=m_AB(:,10,:);
        Lp=m_AB(:,11,:);
        M=m_AB(:,12,:);
        Mp=m_AB(:,13,:);
        J2m=m_AB(:,14,:);
        H2m=m_AB(:,15,:);
        Ks2m=m_AB(:,16,:);


        ind_nan=find(isnan(m_AB)==1);
        ind_inf=find(isinf(m_AB)==1);
        m_AB(ind_nan)=999.0;
        m_AB(ind_inf)=999.0;

        % Write results to output file
        % ----------------------------
        fid1=fopen([outdir '/' epoch_name '_generic_ABmag.dat'],'a');
        fprintf(fid1,[epoch_format_start '%9.4f\t %9.4f\t %9.4f\t ' ...
            '%9.4f\t %9.4f\t %9.4f\t %9.4f\t %9.4f\t %9.4f\t %9.4f\t '...
            '%9.4f\t %9.4f\t %9.4f\t %9.4f\t %9.4f\t %9.4f\t' ...
            epoch_format_end], [epoch_extra_start m_AB(1,1) m_AB(1,2) ...
            m_AB(1,3) m_AB(1,4) m_AB(1,5) m_AB(1,6) m_AB(1,7) m_AB(1,8) ...
```

```
            m_AB(1,9) m_AB(1,10) m_AB(1,11) m_AB(1,12) m_AB(1,13) ...
            m_AB(1,14) m_AB(1,15) m_AB(1,16) epoch_extra_end]);
        fclose(fid1);
        if multi_spectra == 1
            fid2=fopen([outdir '/generic_ABmag.dat'],'a');
            fprintf(fid2,[master_format_start '%9.4f\t %9.4f\t %9.4f\t '...
                '%9.4f\t %9.4f\t %9.4f\t %9.4f\t %9.4f\t %9.4f\t '...
                '%9.4f\t %9.4f\t %9.4f\t %9.4f\t %9.4f\t %9.4f\t %9.4f\t' ...
                master_format_end], [master_extra_start m_AB(1,1) ...
                m_AB(1,2) m_AB(1,3) m_AB(1,4) m_AB(1,5) m_AB(1,6) ...
                m_AB(1,7) m_AB(1,8) m_AB(1,9) m_AB(1,10) m_AB(1,11) ...
                m_AB(1,12) m_AB(1,13) m_AB(1,14) m_AB(1,15) m_AB(1,16) ...
                master_extra_end]);
            fclose(fid2);
        end
    otherwise
        disp('Something is wrong')
end
```

C.2 SED Fit

C.2.1 SEDfitter.m

```
clc
clear all
close all
import_Whitelock_info
import_tabelb1
load('WISE.mat')
load('NIRCam.mat')
load('MIRI.mat')
Dist = Dist*10^3; %in pc

plot_save = 1; % set to 1 to save a plot on format ObjName.m4v
Movie = 1;   % set to 1 to save a movie on format ObjName.m4v

for White = 1:20
    clear i j h k l w1mpro_ep w2mpro_ep w3mpro_ep w4mpro_ep Pot_Mod ...
        Pot_Mod_Error Mod_Index
    import_Whitelock_object

    CurrObjName = char(ObjName(White));

    AV = AvCorr(White);



    JWST = [F070W F090W F115W F150W F200W F277W F356W F444W F560W F770W ...
        F1000W F1130W F1280W F1500W F1800W F2100W];
    wave_JWST = [wave_NIRCam wave_MIRI];

    bad_data_remover

    % Vega to AB
    w1mpro_ep = w1mpro_ep + 2.683;
    w2mpro_ep = w2mpro_ep + 3.319;
    w3mpro_ep = w3mpro_ep + 5.242;
    w4mpro_ep = w4mpro_ep + 6.604;

    % Apparaent to aboslute magnitude
    W1M = w1mpro_ep+5-5*log10(Dist(White))-AV;
    W2M = w2mpro_ep+5-5*log10(Dist(White));
    W3M = w3mpro_ep+5-5*log10(Dist(White));
    W4M = w4mpro_ep+5-5*log10(Dist(White));



    W1M_mean = mean(W1M);
```

```
    W2M_mean = mean(W2M);
    W3M_mean = mean(W3M);
    W4M_mean = mean(W4M);


    SED_observed = [W1M W2M W3M W4M];
    SED_observed_mean = [W1M_mean W2M_mean W3M_mean W4M_mean];

    Pot_Mod = zeros(1,size(SED_observed,1));
    Pot_Mod_Error = zeros(1,size(SED_observed,1));

    if Movie == 1
        v = VideoWriter(strcat('ABmagsV4/figures/SED_fit/Movies/', ...
            CurrObjName, '.m4v'),'MPEG-4');
        v.FrameRate = 2;
        open(v)
    end
    %% Fit the SED
    fig1 = figure('position',[100 100 850 600]);
    for j = 1:size(SED_observed,1)
        [A,Mod_Index] = min(abs(W1-W1M(j)+W2-W2M(j)+W3-W3M(j)+W4-W4M(j)));
        Pot_Mod(j) = Mod_Index;
        i = Mod_Index;
        plot(wave_WISE,[W1(i) W2(i) W3(i) ...
            W4(i)],'-*r',wave_WISE,SED_observed(j,:),'-ko')
        axis([0 25 -10 5])
        legend(['WISE Model #' num2str(Model(i))],'WISE Observation')
        ylabel('M_{AB}')
        xlabel('Wavelength (micron)')
        grid on
        title([CurrObjName ' Observation #' num2str(j)])
        set(gca,'YDIR','reverse','FontSize',16)
        drawnow
        if Movie == 1
            writeVideo(v,getframe(fig1))
            M(i) = getframe(fig1);
        end
        Pot_Mod_Error(j) = mean(abs([W1(i) W2(i) W3(i) ...
            W4(i)]-SED_observed(j,:)));
    end
    if Movie == 1
        close(v)
        close all
    end
    %% Create result figure
    fig2 = figure('position',[100 100 850 600]);
    modeMod = mode(Pot_Mod);
    numberofMod = find(Pot_Mod == modeMod);
    if length(numberofMod) > 1
        j = find(Pot_Mod == modeMod,1);
    else
```

```
            j = find(Pot_Mod_Error == min(Pot_Mod_Error));
        end
        subplot(2,1,1)
        Pot_Mod(j) = Mod_Index;
        i = Mod_Index;
        plot(wave_WISE,[W1(i) W2(i) W3(i) ...
            W4(i)],'-*r',wave_WISE,SED_observed(j,:),'-ko')
        axis([0 25 -10 0])
        legend(['WISE Model #' num2str(Model(i))],'WISE Observation')
        ylabel('M_{AB}')
        xlabel('Wavelength (micron)')
        title([CurrObjName ' - Best fit'])
        set(gca,'YDIR','reverse','FontSize',16)
        subplot(2,1,2)
        k = find(Model==Model(Pot_Mod(j)));
        for o=k(1):k(end)
            plot(wave_WISE,[W1(o) W2(o) W3(o) W4(o)],'*r')
            hold on
        end
        for l=1:size(SED_observed,1)
            plot(wave_WISE,SED_observed(l,:),'ko')
        end
        axis([0 25 -10 0])
        ylabel('M_{AB}')
        xlabel('Wavelength (micron)')
        set(gca,'YDIR','reverse','FontSize',16)
        hold off
        if plot_save == 1
            saveas(gcf,['ABmagsV4/figures/SED_Fit/WISE_FIT_' ...
                num2str(WhiteNumber(White)) '_' CurrObjName '_MOD' ...
                num2str(Model(i)) '_SED.eps'])
        end

        %% Display model info
        disp(['Model: ' num2str(Model(i))])
        disp(['Teff: ' num2str(Teff(i)) ' K'])
        disp(['Mass: ' num2str(Mass(i)) ' M_sun'])
        disp(['LogL: ' num2str(logL(i)) ' L_sun'])
        disp(['Cex: ' num2str(Cex(i)) ' log(C-O)+12'])
        disp(['Class: ' char(Class(Model(i)))])
        disp(['LogMdot: ' num2str(logMdot(Model(i))) ' M_sun/year'])

        %% Save fit info
        fid1=fopen(['ABmagsV4/figures/SED_Fit/WISE_FIT_' ...
            num2str(WhiteNumber(White)) '_' CurrObjName '_MOD' ...
            num2str(Model(i)) '_SED.txt'],'w');
        fprintf(fid1,'%s \r\n',['Object: ' CurrObjName]);
        fprintf(fid1,'%s \r\n',['Type: ' char(Type(White))]);
        fprintf(fid1,'%s \r\n',['Distance: ' num2str(Dist(White)) ' pc']);
        fprintf(fid1,'%s \r\n','-------------------');
        fprintf(fid1,'%s \r\n',['Model: ' num2str(Model(i))]);
```

```
    fprintf(fid1,'%s \r\n',['Teff: ' num2str(Teff(i)) ' K']);
    fprintf(fid1,'%s \r\n',['Mass: ' num2str(Mass(i)) ' M_sun']);
    fprintf(fid1,'%s \r\n',['LogL: ' num2str(logL(i)) ' L_sun']);
    fprintf(fid1,'%s \r\n',['Teff: ' num2str(Teff(i)) ' K']);
    fprintf(fid1,'%s \r\n',['Cex: ' num2str(Cex(i)) ' log(C-O)+12']);
    fprintf(fid1,'%s \r\n',['Class: ' char(Class(Model(i)))]);
    fprintf(fid1,'%s \r\n',['LogMdot: ' num2str(logMdot(Model(i))) ' ...
        M_sun/year']);
    fprintf(fid1,'%s \r\n','   W1     W2        W3      W4      [AB_mag] ...
        (Observed, Model)');
    fprintf(fid1,'%2.4f  %2.4f   %2.4f  %2.4f\r\n',[W1M(j) W2M(j) W3M(j) ...
        W4M(j)]);
    fprintf(fid1,'%2.4f  %2.4f   %2.4f  %2.4f\r\n',[W1(i) W2(i) W3(i) W4(i)]);
end
```

C.2.2 bad_data_remover.m

```
%% Removes NaN and high chi^2 from WISE data
%  Adam Hjort 2016

% Remove NaN from data
Nan_check = ~isnan(w1mpro_ep+w2mpro_ep+w3mpro_ep+w4mpro_ep);
w1mpro_ep = w1mpro_ep(Nan_check);
w1rchi2_ep = w1rchi2_ep(Nan_check);
w2mpro_ep = w2mpro_ep(Nan_check);
w2rchi2_ep = w2rchi2_ep(Nan_check);
w3mpro_ep = w3mpro_ep(Nan_check);
w3rchi2_ep = w3rchi2_ep(Nan_check);
w4mpro_ep = w4mpro_ep(Nan_check);
w4rchi2_ep = w4rchi2_ep(Nan_check);

% Remove high reduced chi^2
rchi2 = 5; % Select reduced chi^2 value

rchi2_check = find(w1rchi2_ep<rchi2 & w2rchi2_ep<rchi2 & w3rchi2_ep<rchi2 ...
    & w4rchi2_ep<rchi2);
w1mpro_ep = w1mpro_ep(rchi2_check);
w1rchi2_ep = w1rchi2_ep(rchi2_check);
w2mpro_ep = w2mpro_ep(rchi2_check);
w2rchi2_ep = w2rchi2_ep(rchi2_check);
w3mpro_ep = w3mpro_ep(rchi2_check);
w3rchi2_ep = w3rchi2_ep(rchi2_check);
w4mpro_ep = w4mpro_ep(rchi2_check);
w4rchi2_ep = w4rchi2_ep(rchi2_check);
```

Appendix D

WISE objects

Number	Object Name	Dist	A_V	$A_{3.31}$	Type	$\log\dot{M}_{Obs}$	Comment
1	[TI98]0418+0122	6.42	0.37	0.021699862	Mi	-5.73	
2	V617 Mon	2.94	1.01	0.059234758	C	-5.96	Binary
3	RT Gem	3.43	0.54	0.031670069	C	N/A	
4	CG Mon	1.99	0.75	0.043986207	C	N/A	
5	V471 Pup	4.17	1.43	0.083867034	Sr	N/A	Binary
6	FF Pup	3.77	0.58	0.034016	C	N/A	
7	[ABC89]Ppx19	5.89	2.19	0.128439723	C	N/A	
8	[ABC89]Ppx40	5.13	1.54	0.090318344	C	N/A	
9	[ABC89]Vel44	4.18	3.34	0.19588524	Mi	N/A	
10	TV Vel	1.84	1.08	0.063340137	C	N/A	
11	[ABC89]Car87	7.09	3.46	0.202923033	Mi	N/A	
12	[W65] c13	5.38	4.53	0.265676688	Mi	N/A	
13	[ABC89]Cen4	4	1.68	0.098529103	C	N/A	
14	[ABC89]Cen32	4.4	2.58	0.151312551	Mi	-5.45	
15	CF Cru	5.88	5.8	0.340159997	C	N/A	
16	[ABC89]Cir26	3.81	4.11	0.241044412	Mi	N/A	
17	CGCS3721	2.71	1.29	0.075656275	C	N/A	
18	SZ Ara	1.29	1.19	0.069985047	C	N/A	
19	[TI98]2259+1249	4.15	0.49	0.028737655	C	-5.88	
20	[TI98]2223+2548	2.84	0.16	0.009383724	C	-5.94	

Table D.1: List of objects from Whitelock et al. (2006) that could be used with data from the AllWISE Multiepoch Photometry Database. *Mi* is short for Mira variable star, *C* is short for Carbon star and *SR* is short for SemiRegular variable star. The value in $\log\dot{M}_{Obs}$ is the observed mass loss given in $M_{\odot}$ / year.